© 2016. Published by The Company of Biologists Ltd | Development (2016) 143, 623-634 doi:10.1242/dev.127993

RESEARCH ARTICLE

Modulation of junction tension by tumor suppressors and proto-oncogenes regulates cell-cell contacts

Floris Bosveld[§], Boris Guirao, Zhimin Wang, Mathieu Rivière*, Isabelle Bonnet[‡], François Graner* and Yohanns Bellaïche[§]

ABSTRACT

Tumor suppressors and proto-oncogenes play crucial roles in tissue proliferation. Furthermore, de-regulation of their functions is deleterious to tissue architecture and can result in the sorting of somatic rounded clones minimizing their contact with surrounding wild-type (wt) cells. Defects in the shape of somatic clones correlate with defects in proliferation, cell affinity, cell-cell adhesion, oriented cell division and cortical contractility. Combining genetics, live-imaging, laser ablation and computer simulations, we aim to analyze whether distinct or similar mechanisms can account for the common role of tumor suppressors and proto-oncogenes in cell-cell contact regulation. In *Drosophila* epithelia, the tumor suppressors Fat (Ft) and Dachsous (Ds) regulate cell proliferation, tissue morphogenesis, planar cell polarity and junction tension. By analyzing the evolution over time of *ft* mutant cells and clones, we show that *ft* clones reduce their cell-cell contacts with the surrounding wt tissue in the absence of concomitant cell divisions and over-proliferation. This contact reduction depends on opposed changes of junction tensions in the clone bulk and its boundary with neighboring wt tissue. More generally, either clone bulk or boundary junction tension is modulated by the activation of Yorkie, Myc and Ras, yielding similar contact reductions with wt cells. Together, our data highlight mechanical roles for proto-oncogene and tumor suppressor pathways in cell-cell interactions.

KEY WORDS: Fat/Dachsous and Hippo pathways, Myc, Ras, Junction tension, Myosins, Clone shape

INTRODUCTION

Tumor suppressors and oncogenes play fundamental functions in cell proliferation, growth and apoptosis. The analyses of these functions have led to important advances in our understanding of tissue development and homeostasis as well as pathologies, including tumorigenesis (for reviews, see Zhao et al., 2011; Patel and Edgar, 2014; Baillon and Basler, 2014). In *Drosophila*, analysis of the sizes and shapes of somatic clones affecting tumor suppressor and proto-oncogene activities is instrumental to understanding their contribution in tissue morphogenesis, organization and homeostasis (Resino et al., 2002; Baena-Lopez et al., 2005; Mao et al., 2011; Wartlick et al., 2011; Kuchen et al., 2012; Worley et al., 2013; Restrepo et al., 2014; Heemskerk et al., 2014). Accordingly, somatic mutant clones are essential for unveiling how tumor suppressor and proto-oncogene activities modulate tissue proliferation, growth, cell-cell interactions and cell competition (for a review, see Wagstaff et al., 2013). In particular, the functions of tumor suppressors and proto-oncogenes in tissue organization and morphogenesis have often been recognized as their respective loss and gain of function leads to the formation of a rounded group of mutant cells (somatic clones) having a smooth boundary with the surrounding wild-type (wt) cells and thus reducing their contacts with neighboring wt tissue (Justice et al., 1995; Prober and Edgar, 2000, 2002; Baena-Lopez et al., 2005; Mao et al., 2006; Worley et al., 2013). This property is shared by the Ras and Myc proto-oncogenes as well as components of the Fat/Dachsous (Ft/Ds) and Hippo pathways (Justice et al., 1995; Adler et al., 1998; Johnston et al., 1999; Prober and Edgar, 2000, 2002; Garoia et al., 2000; Baena-Lopez et al., 2005; Mao et al., 2011; Worley et al., 2013).

Experimental and modeling approaches converged to show that the cell-cell contacts between two cell populations can be modulated by cell-cell adhesion, cell cortical contractility and cell division rate and orientation; in particular, the analysis of tissue or compartment boundary formation has provided important insights into the mechanisms modulating cell-cell contacts between two cell populations in response to cell signaling (for a review, see Fagotto et al., 2013). An increase in cell junction tension (which is larger when cortical contractility increases or adhesion decreases) at the interface between two tissues is known to favor a straight boundary between these two tissues or two compartments within a tissue and is essential for tissue development (Graner, 1993; Brodland, 2002; Käfer et al., 2007; Krieg et al., 2008; Hilgenfeldt et al., 2008; Landsberg et al., 2009; Monier et al., 2010; Aliee et al., 2012; Röper, 2012; Fagotto et al., 2013; Calzolari et al., 2014; Umetsu et al., 2014). Theoretical analysis shows that randomly oriented cell divisions induce diffusive random cell displacements (Ranft et al., 2010), thereby adding a slight amount of disorder between two cell populations (Block et al., 2007; Radszuweit et al., 2009). Experimental analyses of cell division rate and orientation demonstrated that an increase in cell junction tension is necessary to prevent disorder introduced by cell divisions occurring near the anterior-posterior parasegment boundary of the *Drosophila* embryo (Monier et al., 2010). Although the role of cell division rate at the *Drosophila* dorsal-ventral boundary of the wing imaginal disc remains a matter of debate, cell division orientation has been shown to contribute to its shaping (Aliee et al., 2012). Cell divisions oriented perpendicular to the boundary can increase the number of cell junctions at the boundary, and hence its raggedness, whereas cell divisions parallel to the boundary can decrease its raggedness. Notably, these effects of cell divisions can be reinforced or conversely weakened according to the number and orientation of cell rearrangements following the divisions.

Polarity, Division and Morphogenesis Team, Institut Curie, CNRS UMR 3215, INSERM U934, 26 rue d'Ulm, 75248 Paris, Cedex 05, France.
*Present address: Matière et Systèmes Complexes, Université Paris Diderot, CNRS UMR 7057, 10 rue Alice Domon et Léonie Duquet, 75205 Paris, Cedex 13, France.
[‡]Present address: Laboratoire Physico-Chimie Curie, Institut Curie, CNRS UMR 168, Université Pierre et Marie Curie, 26 rue d'Ulm, 75248 Paris, Cedex 05, France.

[§]Authors for correspondence (floris.bosveld@curie.fr; yohanns.bellaiche@curie.fr)

Received 5 July 2015; Accepted 7 January 2016

Development (2016) 143, 623-634 doi:10.1242/dev.127993

We initially aimed to understand how Ft/Ds pathway, which modulates the activity of the myosin Dachs and of the Hippo/Yorkie pathway, promotes somatic clone rounding (Mao et al., 2006, 2011; Cho et al., 2006). The tumor suppressors Ft and Ds encode large proto-cadherins that interact in a heterophilic manner and regulate proliferation via the Hippo/Yki pathway or mitochondrial metabolism, planar cell polarity and tissue morphogenesis by promoting oriented cell divisions and cell-cell rearrangements (Mahoney et al., 1991; Clark et al., 1995; Matakatsu and Blair, 2004; Baena-Lopez et al., 2005; Cho et al., 2006; Silva et al., 2006; Willecke et al., 2006; Harvey and Tapon, 2007; Mao et al., 2011; Donoughe and DiNardo, 2011; Bosveld et al., 2012; Brittle et al., 2012; Marcinkevicius and Zallen, 2013; Lawrence and Casal, 2013; Matis and Axelrod, 2013; Degoutin et al., 2013; Sing et al., 2014). Within tissues, opposing gradients of Ds and the Golgi resident kinase Four-jointed, which regulates Ft-Ds interaction, result in the planar polarization of Ft and Ds (Ishikawa et al., 2008; Brittle et al., 2010, 2012; Simon et al., 2010; Bosveld et al., 2012; Ambegaonkar et al., 2012). One of the effectors of Ft and Ds planar polarization is Dachs, which regulates cell division orientation, cell rearrangements, cell affinity, proliferation rate and junction tension (Mao et al., 2006, 2011; Bosveld et al., 2012; Brittle et al., 2012). Dachs membrane localization is promoted by the DHHC palmitoyltransferase Approximated (Matakatsu and Blair, 2008), and is inhibited by the interaction of the F-Box ubiquitin ligase FbxL7 with Ft (Rodrigues-Campos and Thompson, 2014; Bosch et al., 2014). Conversely, the Ds intracellular domain can form a complex with Dachs *in vitro* and Dachs is proposed to be planar polarized in response to Ds polarization on the same cell junction (Bosveld et al., 2012; Brittle et al., 2012). However, it remains to be shown whether the polarization of Ds intracellular domain would be sufficient to polarize Dachs *in vivo*. The loss of Ft or Ds function in mutant clones leads to the formation of rounded clones minimizing their contact with neighboring tissues (Adler et al., 1998; Garoia et al., 2000; Mao et al., 2006). Loss of Ft activity induces apical cell constriction and results in the membrane accumulation of Dachs, and *ft* clone rounding depends on Dachs (Mao et al., 2006, 2011). Whether these changes in Dachs distribution are necessary for *ft* clone rounding remains to be determined.

Here, we investigated the role of loss of tumor suppressor and gain of proto-oncogene function in forming smooth clone boundaries in the *Drosophila* dorsal thorax (notum) epithelium where we could implement a time-lapse approach to follow the dynamics of clones. Initially focusing on the Ft/Ds pathway, we uncovered that *ft* clone rounding originates from two apparently opposed mechanical activities at the clone boundary and in the clone bulk. Extending the analysis to additional tumor suppressors and proto-oncogenes shows how distinct modulations of cell junction tension by tumor suppressors and proto-oncogenes could account for their common role in the regulation of cell-cell contacts.

RESULTS

A time-lapse approach to follow the rounding of *ft* clones

To understand the mechanisms of clone rounding we implemented a time-lapse approach to follow the dynamics of ft^{RNAi} clones within the notum epithelium during pupal development (Fig. 1A). Using a combination of the flip-out and temperature-sensitive Gal4/$Gal80^{ts}$ systems (Basler and Struhl, 1994; McGuire et al., 2001), the clones marked by the expression of membrane-CherryFP (UAS-PH:ChFP) were generated in second instar larvae that were then kept at 18°C to avoid the expression of the UAS-ft^{RNAi}. Following a temperature shift to 29°C at the end of larval development, we compared by time-lapse microscopy the proliferation and the circularity changes of a control group of cells and ft^{RNAi} clones (Fig. 1B-D; Movie 1). As a reporter of Ft activity we imaged Dachs:GFP (D:GFP), membrane levels of which increase upon loss of Ft function (Bosveld et al., 2012). At 10 hours after pupa formation (hAPF), the control and ft^{RNAi} clones had similar circularities and distributions of D:GFP. At 40 hAPF, whereas the control clones exhibited a reduced circularity and a D:GFP distribution similar to the surrounding cells, the ft^{RNAi} clones had a much higher circularity and an increased D:GFP level at cell junctions (Fig. 1B-D). This shows that our live-imaging approach is suitable for understanding how Ft/Ds signaling regulates tissue organization. To investigate whether clone rounding depends on cell division, we compared the respective timing of cell division and clone shape changes as well as the rates of proliferation in control and ft^{RNAi} clones (Fig. 1C). In both control and ft^{RNAi} clones, a wave of cell divisions occurred between 15 and 20 hAPF. During this wave neither the control nor the ft^{RNAi} clones rounded up. In fact, ft^{RNAi} clone rounding was observed after cell divisions had ceased and once D:GFP had started to accumulate (Fig. 1B). Furthermore, the proliferation rates were similar in control and ft^{RNAi} clones, showing that clone rounding can take place in the absence of over-proliferation (Fig. 1C). Together, these data show that rounding of ft^{RNAi} clones, and thus the reduction of their contacts with neighboring wt cells, is not concomitant with cell divisions and does not require a change in proliferation rate.

Dachs exhibits two distinct distributions in *ft* mutant clones

Having found that D:GFP accumulates in ft^{RNAi} clones during rounding and knowing that Dachs is necessary for *ft* clone rounding (Mao et al., 2006, 2011), we performed a detailed analysis of the distribution and the mechanisms of Dachs localization in *ft* clones. Ft signaling is known to prevent Dachs membrane accumulation (Mao et al., 2006, 2011; Bosveld et al., 2012; Brittle et al., 2012). Accordingly, D:GFP levels were increased in *ft* cells and sometimes segregated in distinct regions of the cell junctions (Fig. 2A; Figs S1, S2). We also noticed that D:GFP was strongly enriched all around the circumference of *ft* clones, i.e. at the interface between wt and *ft* cells, but reduced at the transversal junctions (Fig. 1B; Fig. 2A, yellow arrowheads). Quantitative analyses of the D:GFP distribution at clone boundary and transversal junctions revealed that D:GFP within mutant cells neighboring wt cells specifically accumulated at the clone boundary (hereafter referred to as 'Dachs polarization at clone boundary') (Fig. 2J). We therefore investigated the mechanisms leading to the polarization of D:GFP at the *ft* clone boundary. In agreement with the facts that the Ds intracellular domain forms a complex with Dachs *in vitro*, that Ds polarization promotes Dachs polarization and that Ds:GFP is polarized at the boundary of *ft* clones (Fig. 2B, yellow arrowheads; Strutt and Strutt, 2002; Ma et al., 2003; Matakatsu and Blair, 2004; Bosveld et al., 2012), D:GFP polarization was reduced at the boundary between wt and *ft ds* double mutant cells (Fig. 2C, white arrowheads; Fig. 2J). Whereas the overexpression of a full-length Ds transgene in *ft ds* clones (*ds ft* ds^{UP}) restores D:GFP polarization at the clone boundary (Fig. 2D, yellow arrowheads; Fig. 2J), overexpression of the Ds intracellular domain (Ds:intra) did not (Fig. 2E, white arrowheads; Fig. 2J), suggesting that the extracellular heterophilic Ds-Ft interaction is required to polarize Dachs. Accordingly, D:GFP polarization was reduced at the clone interface of *ds ft* ds^{UP} clones, which abutted a *ft* hypomorphic mutant tissue (compare Fig. 2D and 2F; Fig. 2J). Because loss of Ft activity inhibits Dachs membrane levels, D:GFP is also elevated in *ft* cells surrounding *ds ft* ds^{UP} clones. Together, our results support the hypothesis that Dachs is

Development (2016) 143, 623-634 doi:10.1242/dev.127993

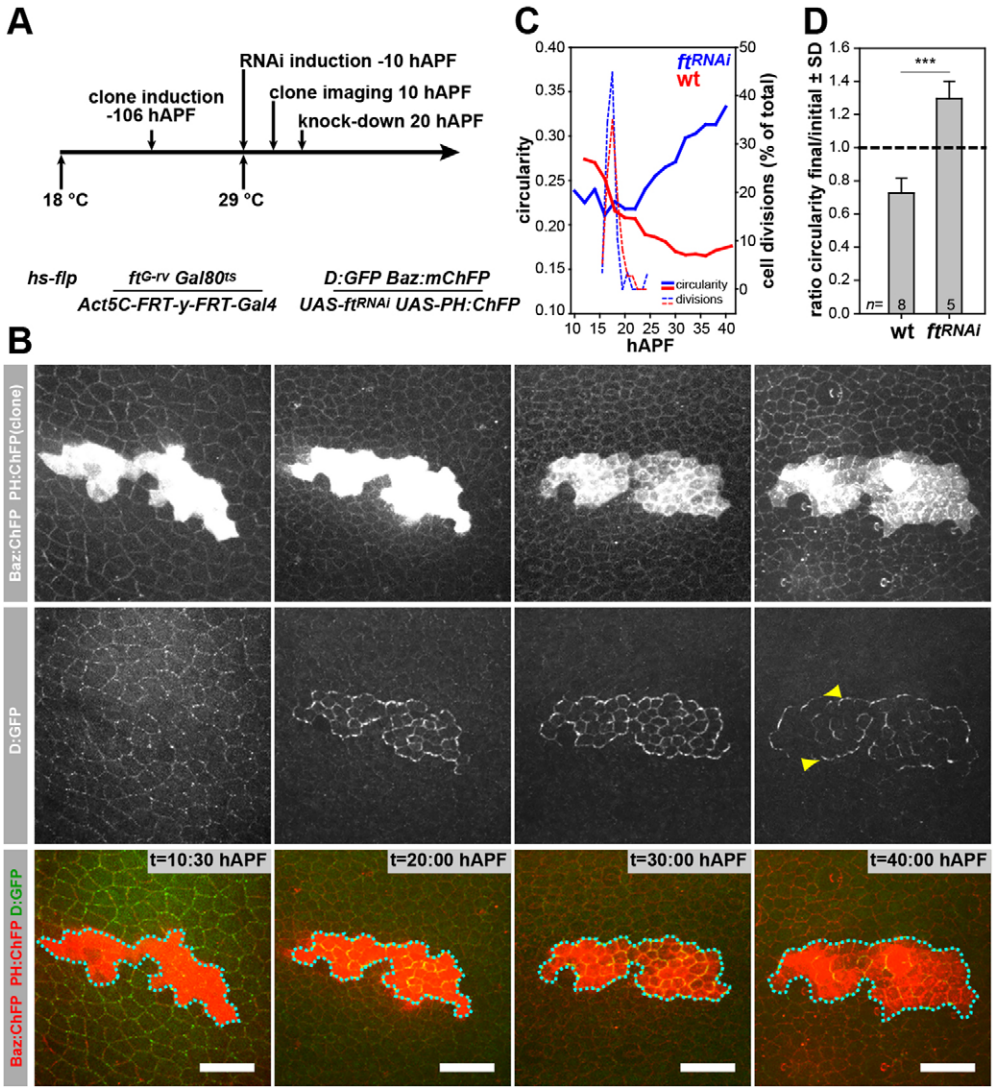

Fig. 1. Cell division and over-proliferation does not account for the increased circularity of *ft* clones. (A) Schematic illustrating the dynamics of Ft loss-of-function clones in pupa of the indicated genotype. Embryos and larvae were raised at 18°C for 7 days. Upon a 7-min heat-shock at 37°C larvae were returned to 18°C. After 4-5 additional days at 18°C, late third instar larvae were transferred to 29°C to induce expression of the *ft* dsRNA. After 22±4 h at 29°C 10 hAPF pupae were mounted and imaged at 29°C. Strong downregulation of Ft function, measured by increase in D:GFP relative to surrounding tissue, is observed at ∼20 hAPF (see B). (B) Images of Movie 1 showing a ft^{RNAi} clone labeled by PH:ChFP in a tissue expressing Baz:mChFP (white in top panels; red in bottom panels) and D:GFP (white in middle panels; green in bottom panels). Cyan dashed lines indicate clone boundaries. At 10:30 (h:min) hAPF, D:GFP localization is similar inside and outside of the ft^{RNAi} clone. At ∼20 hAPF, D:GFP is enriched in the ft^{RNAi} clone. Over time, D:GFP gradually accumulates and becomes polarized at the clone boundary. This clone becomes rounder over time (see C). Yellow arrowheads indicate cells where D:GFP is polarized. Scale bars: 20 µm. (C) Circularity (solid lines) and number of divisions (dashed lines) versus time for a wt clone (red) and the ft^{RNAi} clone (blue) shown in B. (D) Mean ratio of final/initial clone circularity of wt and ft^{RNAi} clones. ***P<0.0005 (t-test); n, clone numbers; error bars represent s.d.

not only enriched in *ft* mutant clones, but is also polarized at the clone boundary due to Ds polarization.

Two independent and complementary results strengthen the proposal that the polarization of the Ds intracellular domain is sufficient to polarize Dachs at the *ft* clone boundary. First, *in vitro* analyses of D:GFP polarization using an S2-induced polarity assay (Johnston et al., 2009; Ségalen et al., 2010), in which the extracellular and transmembrane domains of the homophilic adhesion molecule Echinoid are fused to the intracellular domain of Ds (Ed:mCh:Ds:intra), showed that the Ed:mCh:Ds:intra polarity domain was sufficient for D:GFP recruitment and polarization, which colocalized with Ed:mCh:Ds:intra (Fig. 2K). Second, within the tissue, we found that the circumference of clones that overexpressed a chimera of the Ds intracellular and Ft extracellular domains (Casal et al., 2006) in *ds ft* clones (*ds ft ds:intra:ft:extra*^{UP}) can harbor a D:GFP polarization at the clone interface (Fig. 2G, yellow arrowheads; Fig. 2J). Such polarization was lost in *ds:intra:ft:extra*^{UP} cells surrounded by *ds* cells (*ds ft ds:intra:ft:extra*^{UP} in *ds*; compare Fig. 2G and 2H; Fig. 2J), indicating that the polarization of the Ds intracellular domain appears to be sufficient to polarize Dachs independently of the orientation of the Ft-Ds extracellular heterophilic interaction. Altogether these results indicate that loss of Ft activity induces two distinct Dachs distributions within *ft* clones: an increase of Dachs levels within *ft* cells and a Dachs accumulation at clone boundary junctions in response to Ds intracellular domain polarization.

Two complementary activities of Dachs contribute to *ft* clone rounding

The identification of two distinct changes in Dachs distribution in *ft* clones prompted us to investigate their respective contribution to clone rounding. We previously found that D:GFP polarization at cell junctions correlates with a higher junction tension (Bosveld et al., 2012). To investigate further the role of Dachs polarization in junction tension regulation, we first confirmed that Dachs polarization promotes an increase in junction tension, i.e. the force exerted by the junction parallel to it, which is considered positive when it reduces junction length and which can be estimated by the initial recoil velocity of the junction vertices upon its severing by laser ablation (Hutson et al., 2003). As Ds planar polarization is independent of Dachs function (Fig. 3A-C; Bosveld et al., 2012; Brittle et al., 2012), we compared the relaxation velocity of junctions showing high or low Ds:GFP signal in a *dachs* tissue, the junctions being labeled by Baz:mChFP. The loss of Dachs function abolishes the difference in relaxation velocity between junctions bearing high and low Ds:GFP (Fig. 3D). Because Ds and Dachs are

Development (2016) 143, 623-634 doi:10.1242/dev.127993

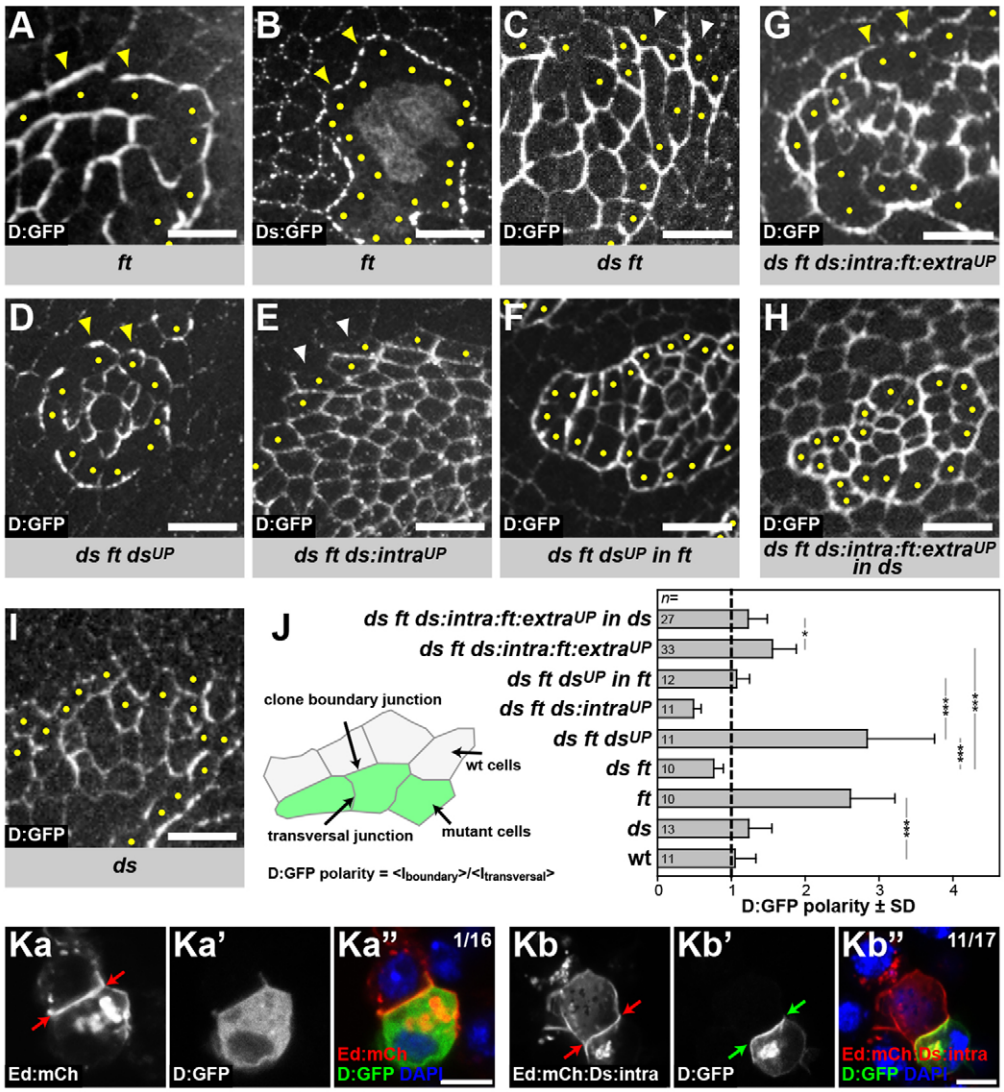

Fig. 2. Dachsous polarizes Dachs at *ft* clone boundaries. (A-I) D:GFP (A,C-I) and Ds:GFP (B) localization in clones and tissues of indicated genotypes. Yellow arrowheads indicate junctions where D:GFP or Ds:GFP are polarized whereas white arrowheads indicate the ones devoid of polarization. Yellow dots indicate mutant cells abutting wt cells. In agreement with previous findings (Ma et al., 2003), Ds staining appears cytoplasmic and diffuse inside the *ft* clone and remains at the membrane at the *ft* clone boundary. The Ft-Ds interaction might be needed to maintain Ds at the membrane (B). (J) Explanation of D:GFP polarity quantification. D:GFP is considered polarized when the ratio of the average junction intensity at clone boundaries ($<I_{boundary}>$) over the average junction intensity at transversal junctions ($<I_{transversal}>$) is >1. Graph shows D:GFP polarization at clone boundaries of indicated genotypes. *P<0.05, ***P<0.0005 (one-way ANOVA Tukey's test); *n*, clone numbers; error bars represent s.d. (Ka-Kb″) D:GFP polarization using an S2 induced polarity assay, in which the extracellular and transmembrane domains of the homophilic adhesion molecule Echinoid are fused to the intracellular domain of Ds (Ed:mCh:Ds:intra). Images of fixed S2 cell aggregates showing the polarized interface between two cells created by homophilic interaction of either Ed:mCh (Ka) or Ed:mCh:Ds:intra (Kb) (red arrows). In each doublet, one cell also expresses D:GFP (Ka′,Kb′). D:GFP does not localize to the polarized interface when co-expressed in cells expressing Ed:mCh (Ka′, Ka″), but is efficiently recruited to the interface when co-expressed with Ed:mCh:Ds:intra (Kb′,Kb″) (green arrows). Numbers in the top corner of Ka″ and Kb″ indicate the proportion of cells with polarized D:GFP (1 out of 16, and 11 out of 17). Scale bars: 10 µm (A-I); 5 µm (Ka″,Kb″).

planar polarized at the same junctions, this indicates that Dachs activity is necessary to increase the tension of junctions harboring Ds and Dachs polarization.

Having confirmed that Dachs polarization is necessary to increase cell junction tension in wt tissue, we tested whether the Dachs polarization at the boundary of *ft* clones and the increase in cell junction tension (Fig. 4A,B; Bosveld et al., 2012) are sufficient to fully explain the higher circularity of *ft* clones relative to wt clones. The increased tension at *ft* clone boundaries was independent of the clone size and the orientation of the ablated junctions (Fig. S3). The loss of Ds activity in *ft* mutant clones is associated with a decreased D:GFP polarization at clone boundaries (Fig. 2C,J) and an average junction tension similar to that of wt (Fig. 4C,C′). Although the circularity of *ds ft* clones was lower than the circularity of *ft* clones, the circularity of *ds ft* clones remained higher than that of wt clones (Fig. 4A). As Dachs activity is essential to increase the *ft* clone boundary tension and the circularity of *ft* clones (Fig. 4A,B; Mao et al., 2006), this indicates that Dachs polarization at the clone boundary increases the circularity of *ft* clones and that an additional Dachs-dependent mechanism inside the clone contributes to *ft* clone rounding (Fig. 1; Fig. 4A).

To identify this additional mechanism, we probed the tension of junctions inside *ft* clones. Unexpectedly, we observed that inside *ft* clones the average cell junction tension was reduced (Fig. 4B). A

Development (2016) 143, 623-634 doi:10.1242/dev.127993

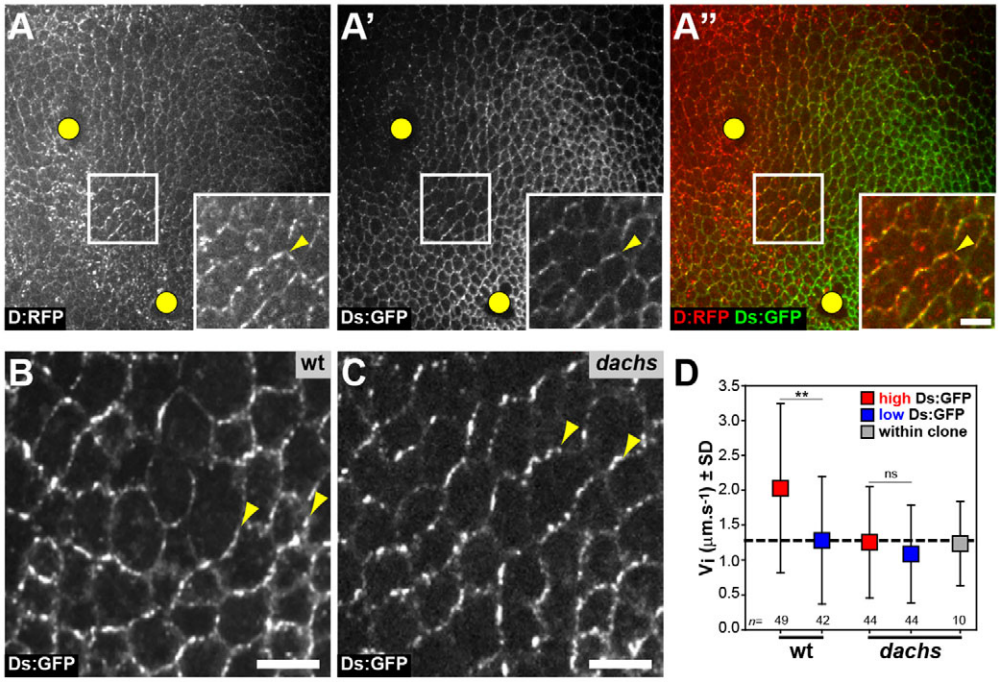

Fig. 3. Dachs regulates cell junction tension. (A-A″) Images of a right hemi-scutellum (posterior notum) tissue expressing D:RFP (white in A; red in A″) and Ds:GFP (white in A′; green in A″) at 18 hAPF. Insets show magnifications of the boxed regions. Yellow arrowheads indicate junctions where D:RFP and Ds:GFP are polarized. Yellow circles mark macrochaetae. In agreement with previous findings (Bosveld et al., 2012), D:RFP and Ds:GFP are planar polarized and colocalize within a restricted domain. This domain corresponds to the area where the *ds* and *fj* gene expression gradients overlap (Bosveld et al., 2012). Note that D:RFP tends to aggregate in small punctate structures. (B,C) Images of posterior notum tissue expressing Ds:GFP in wt (B) and *dachs* (C) tissue. Yellow arrowheads indicate junctions where Ds:GFP is polarized. (D) Tension changes determined by mean initial recoil velocity of vertices of ablated cell junctions with high (red) or low (blue) Ds:GFP levels within the Ds:GFP polarity domain in wt or *dachs* tissue, as well as within *dachs* clones (gray). ***P*<0.005; ns, not significant (*t*-test); *n*, junction numbers; error bars represent s.d. Scale bars: 5 µm.

lower tension inside the clone was also measured in *ds ft* and in *ds* clones, showing that the tension decrease is independent of Ds function (Fig. 4C,D). Cell junction tension inside *ft dachs*, *ds dachs* and *ds ft dachs* clones as well as their circularities were similar to the wt, indicating that Dachs activity is necessary inside *ft* clones to reduce junction tension (Fig. 4B-D). The changes in junction tension were not associated with changes in the levels of the *Drosophila* Myosin II light chain (Spaghetti Squash, Sqh) at the boundary of or inside *ft* or *ds* clones (Fig. 4E,F; Fig. S4).

A common feature of *ft*, *ds* and double *ds ft* clones is to exhibit a higher level of Dachs (Mao et al., 2006; Brittle et al., 2012; Fig. 2A,I; Fig. S1A,H), which is reported to inhibit Wts (Cho et al., 2006) via Zyxin-dependent or -independent mechanisms (Rauskolb et al., 2011; Gaspar et al., 2015). We uncovered that loss of Wts activity (wts^{RNAi}) leads to clone rounding and to a decrease of junction tension similar to that measured inside *ft*, *ds* or *ds ft* clones (Fig. 4G,H). Furthermore, overexpression of Wts in *ft* clones (*ft* wts^{UP}) partially rescued the rounding of *ft* clones by reducing the polarization of Dachs and the tension at clone boundary junctions (Fig. 4G-J). Finally, the lower tension associated with Wts loss of function might be mediated by the activation of Yki as clones overexpressing Yki (yki^{UP}) are characterized by a junction tension similar to that of wts^{RNAi} (Fig. 4G). yki^{UP} clones display a rounder shape than wts^{RNAi} clones (Fig. 4H), suggesting that overexpression of Yki promotes clone rounding by both tension-dependent and tension-independent mechanisms. Together, these experimental observations indicate that Dachs has two apparently opposed mechanical activities: the polarized Dachs distribution at the boundary of the clone increases junction tension and the Dachs accumulation within the clone bulk decreases junction tension.

Two opposed mechanical activities cooperate to promote clone rounding

Next, we aimed to understand better the impact of differential junction tension, and more specifically to determine how both opposed mechanical activities might cooperate to determine the rounding and thus the segregation of developing clones. Based on a theoretical analysis (Graner, 1993; supplementary materials and methods), we analyzed the competition between the tension of cell junctions at the clone boundary γ_b on the one hand, and the tensions of cell junctions within the clone γ_c, or in the surrounding wt cells γ on the other hand (Fig. 5A). Modeling and experiments are independent of the biological origin of these tensions. This analysis shows that: (1) there is an energy cost associated with the length of the clone boundary when junction tensions (γ,γ_b,γ_c) are different; and (2) the tendency of the clone to round up (decrease contact with wt neighbors), or in contrast to scatter (increase contact with wt neighbors), is determined by the sign and amplitude of the 'dimensionless clone tension' parameter:

$$\sigma = 1/\gamma\{\gamma_b - [(\gamma + \gamma_c)/2]\}. \quad (1)$$

It represents the energy cost per unit length of increasing the clone boundary by changing 'homotypic' junctions (wt-wt or mutant-mutant) into 'heterotypic' boundary junctions (wt-mutant), and should not be confused with the cell junction tensions themselves that are probed with laser ablations. An advantage of this description is that it takes into account junction tensions only with respect to their relative values, which are directly extracted from laser ablation experiments. The expression of σ is general and includes the case where the tensions on both sides of a domain boundary are the same,

Development (2016) 143, 623-634 doi:10.1242/dev.127993

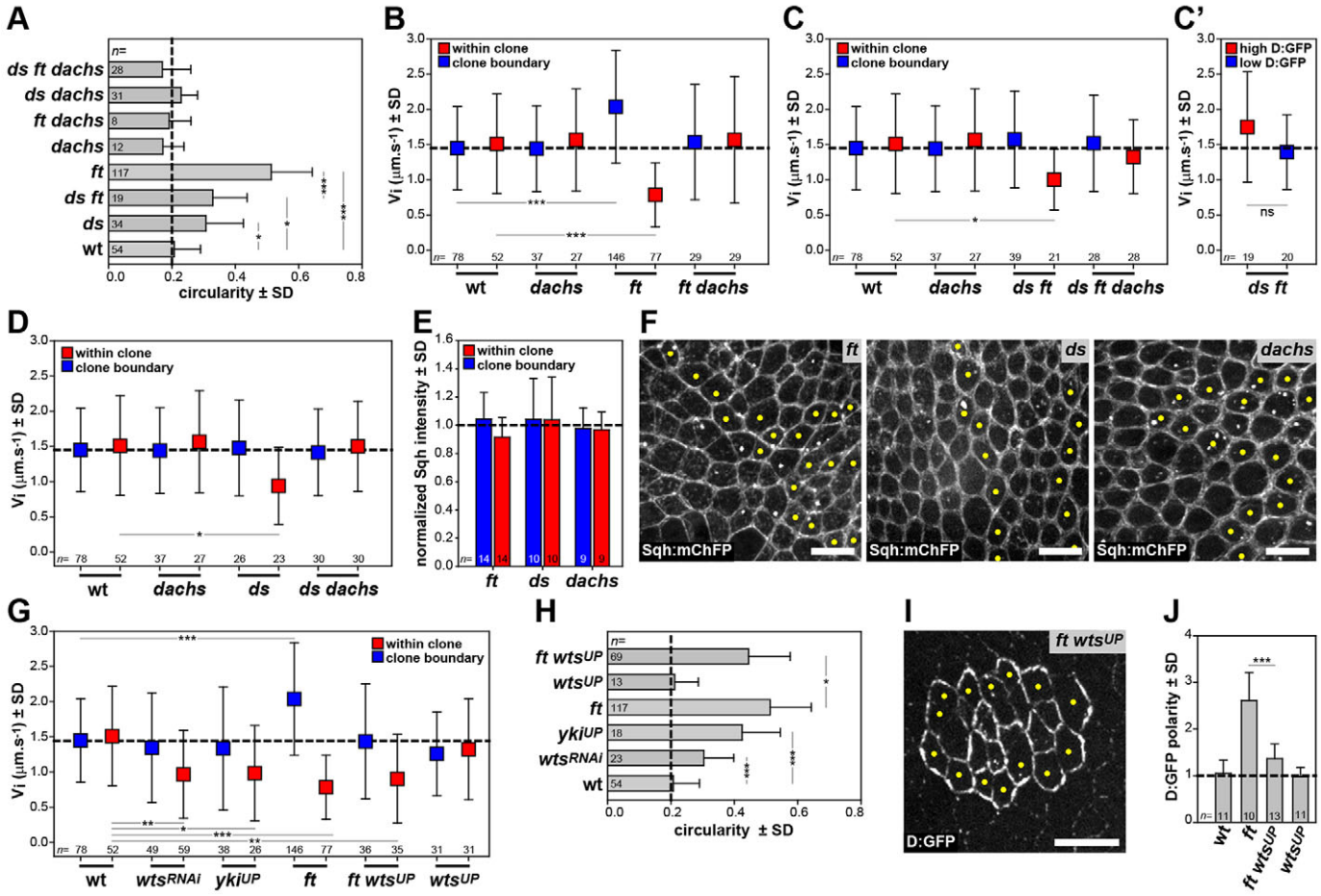

Fig. 4. Dachs has two distinct mechanical activities. (A) Mean clone circularity in the indicated genotypes. (B-D) Mean initial recoil velocity of vertices of ablated cell junctions at clone boundaries (blue) or junctions inside clones (red) of the indicated genotypes (B,C,D) and of junctions with high D:GFP (red) or low D:GFP (blue) at *ds ft* clone boundaries (C′). In *ds ft* clones, the tension of boundary junctions harboring high or low D:GFP are not different (P=0.08, *t*-test). (E) Normalized Sqh:ChFP intensity at clone boundary (blue) and bulk junctions (red) in *ft*, *ds* and *dachs*. (F) Sqh:ChFP localization in *ft* (left), *ds* (middle) and *dachs* (right) mutant clones. Yellow dots mark mutant cells abutting wt cells. (G) Mean initial recoil velocity of vertices of ablated cell junctions at clone boundaries (blue) or junctions inside clones (red) of the indicated genotypes. (H) Mean clone circularity in the indicated genotypes. (I) Image showing D:GFP localization in a *ft* wts^{UP} clone. Yellow dots mark mutant cells abutting wt cells. (J) D:GFP polarization at wt, *ft* and *ft* wts^{UP} clone boundaries. In all graphs, *P<0.05, **P<0.005, ***P<0.0005 (one-way ANOVA Tukey's test for A,H,J; one-way ANOVA Dunnett's test for B,C,D,G); ns, not significant (*t*-test for C′); *n*, clone numbers (A,E,H,J) or junction numbers (B-D,G); error bars represent s.d. Scale bars: 10 µm.

namely $\gamma_c=\gamma$ (Landsberg et al., 2009). It emphasizes that the junction tensions around and within the clone act antagonistically to contribute to the clone boundary energy cost. We therefore expect that when σ is positive, the clone boundary becomes more regular and its circularity increases, thus reducing contact with neighboring wt cells. By contrast, when σ is negative, the heterotypic (wt-mutant) junctions are favored and clones would gradually become more scattered. In between, when σ is null, which corresponds to a wt clone in a wt tissue, we expect it to become slightly more ragged over time (partly as a result of cell division randomly oriented with respect to clone boundary). Importantly, this agrees with our experimental observations: (1) wt clone circularity decreases over time (Fig. 1C); and (2) ft^{RNAi} clone circularity increases over time (Fig. 1C). This is illustrated in the graphs (Fig. 5B,D; Fig. S5B) showing the sign of σ versus the junction tensions at the clone boundary (γ_b) and inside the clone (γ_c) measured in wt, *ft*, *ds*, *ds ft* and wts^{RNAi} clones (Fig. 4B-D,G).

Using numerical simulations, we challenged more quantitatively this modeling by simulating the growth and proliferation of mutant clones using the cellular Potts model directly based on the ratios of experimental tension (Fig. 5C,D; Fig. S5; Movie 3). They showed that: (1) the experimental tension values in wt, *ft*, *ds* and *ds ft* both at clone boundary and inside the clone agree with the rounding of *ft* clones and the lower circularity of *ds* and double *ds ft* clones (Fig. 5D); (2) the combination of an increase of junction tension at the clone boundary and a decrease of junction tension inside the clone leads to a higher circularity than an increase of junction tension solely at the clone boundary (compare ft, simulated using tensions γ_b and γ_c with ft_b, simulated using γ_b and $\gamma_c=\gamma$; Fig. S5B); and (3) the dimensionless clone tension is relevant, and the observed clone circularity increases with σ similarly in experiments and in simulations (Fig. 5D; Fig. S5B). Our experimental observations and modeling of the *ft* clones uncovers how two distinct activities of the myosin Dachs associated with two distinct changes in its localization could induce clone rounding (reducing their contact with neighboring wt cells) by both increasing junction tension at the clone boundary and reducing it inside the clone.

Overexpression of proto-oncogenes modulates junction tension

Having found that the modulation of junction mechanical properties by the Ft/Ds and Hippo/Yki pathways promote clone rounding, we investigated whether the overexpression of proto-oncogenes known

Development (2016) 143, 623-634 doi:10.1242/dev.127993

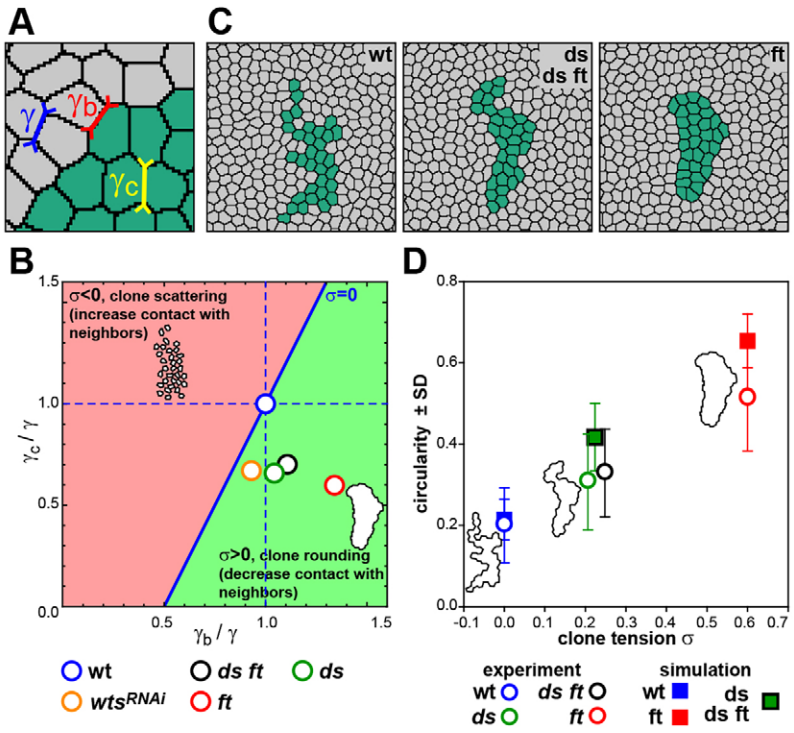

Fig. 5. Balance of cell junction tension accounts for somatic clone rounding. (A) Junction tension parameters used for simulations were: wt (γ, blue), clone boundary (γ_b, red), clone bulk (γ_c, yellow). γ_b/γ and γ_c/γ for each genotype were obtained from average experimental recoil velocities (Fig. 4B-D,G). (B) Parameter space of line tension ratios (γ_b/γ, γ_c/γ) showing regions where clones are expected to scatter (red, σ<0), or to round up (green, σ>0). Blue line (σ=0) separates the two regions and contains the wt clone in a wt tissue (γ_b/γ,γ_c/γ)=(1,1). Note that the domain to which a clone belongs, and its distance to the blue line, which represents its tendency to round up or scatter, solely depend on the sign and value of the dimensionless clone tension σ, respectively. wt: σ=0, *wts*^{RNAi}: σ=0.10, *ds*: σ=0.21, *ds ft*: σ=0.23, *ft*: σ=0.60. (C) Final images of simulated clones (green) using average experimental tension values. Owing to similarities of γ_b and γ_c in *ds* and *ds ft*, their means were used for *ds* and *ds ft* simulations. See Movie 2. (D) Mean clone circularity in experimental (circles) and simulated (squares) clones versus the dimensionless clone tension σ. Clone outlines (C) illustrate clone circularity. Twenty simulations were quantified per condition; error bars represent s.d.

to be associated with clone rounding also modulates junction tension. As previously reported (Prober and Edgar, 2000, 2002), we observed that the overexpression of Myc (*myc*^{UP}) as well as the overexpression of a gain-of-function allele of Ras (*rasV12*^{UP}) promote clone rounding (Fig. 6A). Probing the junction tension at the boundary and inside *myc*^{UP} and *rasV12*^{UP} clones unveiled distinct regulations of bulk or clone boundary junction tension as observed in the case of Ft/Ds or Hippo/Yki pathways (Fig. 6B). Whereas junction tension was reduced inside *myc*^{UP} clones and unchanged at the boundary, the junction tension was unchanged inside *rasV12*^{UP} clones but greatly increased at the boundary. The measured changes in junction tension are compatible with the rounding of somatic clones shown by our computer simulations (Fig. S5B). As the overexpression of Myc and RasV12 are both known to be associated with over-proliferation (Prober and Edgar, 2000, 2002), their distinct impacts on junction tension strongly suggest that over-proliferation cannot be the only cause of their clone rounding. Accordingly, and as observed for the development of Gal4/Gal80^{ts} *ft*^{RNAi} clones, the proliferation rate in Gal4/Gal80^{ts} *rasV12*^{UP} clones was similar to that of control clones, and *rasV12*^{UP} clone rounding was observed after the main cell division wave (Fig. 6C-E). We therefore investigated whether the observed changes in junction tensions and in clone circularities were associated with altered myosin distributions.

In *myc*^{UP} clones, D:GFP was not polarized at the interface of the clone. Furthermore, a heterogeneous D:GFP enrichment was observed at only a few *rasV12*^{UP} clone boundaries, and this enrichment was weak (Fig. 6I,J). Such a weak increase is unlikely to be responsible for the *rasV12*^{UP} clone circularity, which is similar to that of *ft* clones. Moreover, in all experimental conditions, the D:GFP levels were normal inside the clones. We therefore turned our attention to the distribution of MyoII (Sqh:GFP). *rasV12*^{UP} clones were associated with an increase in MyoII localization at the clone boundaries (Fig. 6F,H). Such an increased level of MyoII at the boundary of *rasV12*^{UP} clone is in full agreement with the observed higher tension also reported for the MyoII distribution along the anterior-posterior compartment boundaries or during cell intercalation (Rauzi et al., 2008; Fernandez-Gonzalez et al., 2009; Monier et al., 2010; Umetsu et al., 2014). In contrast to *rasV12*^{UP}, MyoII was globally reduced within *myc*^{UP} clones (Fig. 6F,G). To determine whether the reduction of MyoII levels can account for the rounding of *myc*^{UP} clones, we tested whether mimicking a reduction of MyoII levels using *sqh*^{RNAi} was sufficient to decrease junction tension and to induce a rounded clone shape. Indeed, reducing MyoII levels led to a reduced tension inside *sqh*^{RNAi} clones and promoted clone rounding (Fig. 6A,B).

DISCUSSION

The segregation of tissues or of tissue compartments plays fundamental roles in the regulation of growth, patterning and morphogenesis (for a review, see Fagotto, 2014). Numerous tumor suppressors and proto-oncogenes share the common feature of promoting cell segregation apparent by the rounding of somatic clones upon their loss or gain of functions, respectively (Adler et al., 1998; Johnston et al., 1999; Prober and Edgar, 2000, 2002; Garoia et al., 2000; Baena-Lopez et al., 2005; Mao et al., 2006, 2011; Worley et al., 2013). Here, we show that loss of Ft/Ds and Hippo tumor-suppressor pathways as well as gain of function of the proto-oncogenes Myc, Ras and Yki lead to changes in cell junction tension. Although the changes are distinct and depend on distinct molecular mechanisms, taking into account both clone boundary and bulk tensions is sufficient to account for their segregation from surrounding wt tissue. Although previous works demonstrated that cell cortical contractility or cell adhesion at the interface between two compartments, tissues or clones can promote their separation or contribute to tissue invagination (Graner, 1993; Le Borgne et al., 2002; Brodland, 2002; Wei et al., 2005; Laplante and Nilson, 2006; Landsberg et al., 2009; Monier et al., 2010; Chang et al., 2011; Aliee et al., 2012; Röper, 2012; Fagotto et al., 2013; Calzolari et al., 2014; Umetsu et al., 2014), our genetic and modeling findings show that

Development (2016) 143, 623-634 doi:10.1242/dev.127993

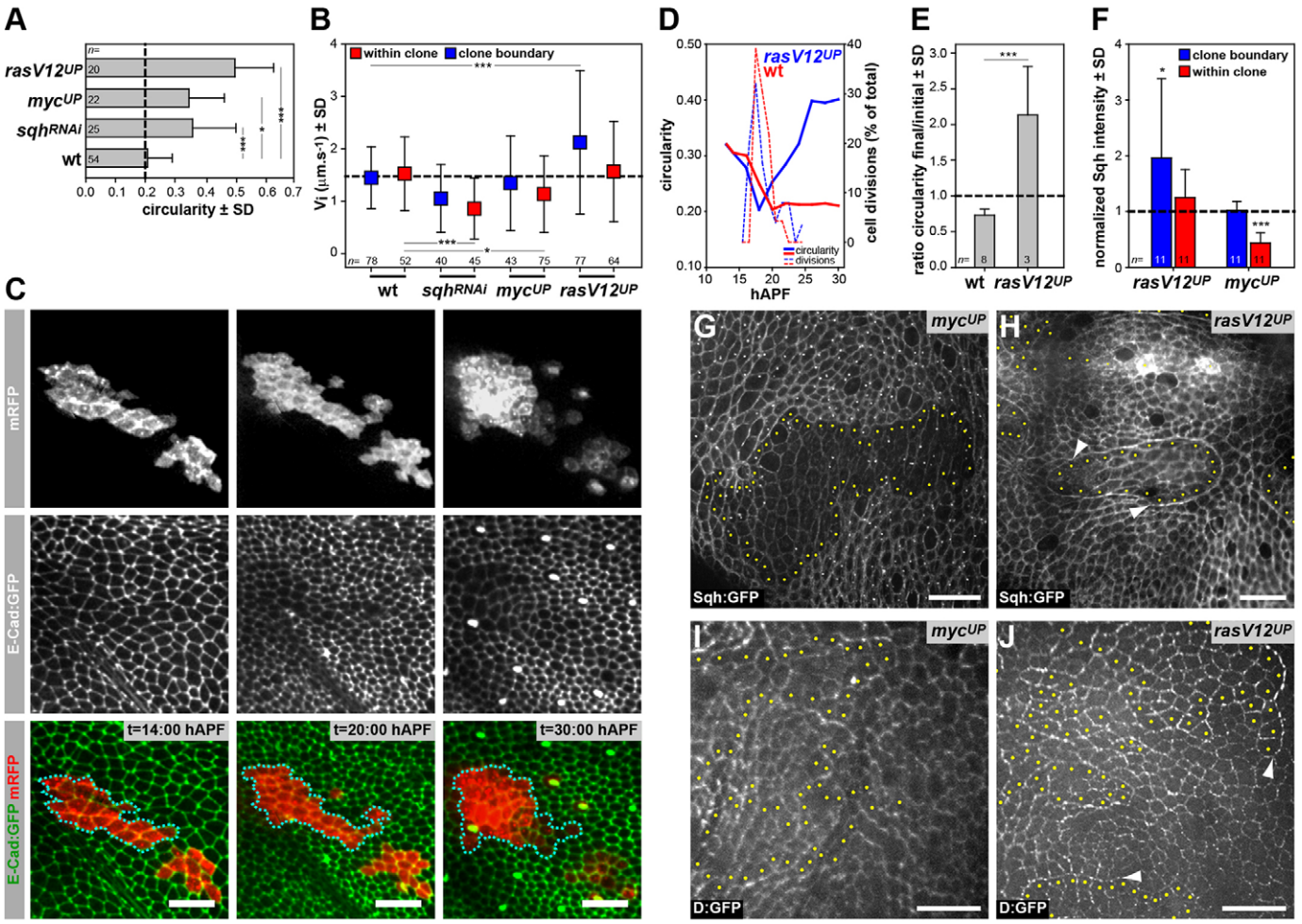

Fig. 6. Proto-oncogene overexpression affects cell junction tension and clone rounding. (A) Mean clone circularity in the indicated genotypes. (B) Mean initial velocity of vertex relaxation after ablation of cell junctions at clone boundaries (blue) or junctions inside clones (red) of the indicated genotypes. (C) Images of Movie 3 showing a *rasV12*^{UP} clone (imaged as in Fig. 1) labeled by mRFP (white in top panels; red in bottom panels) in a tissue expressing E-Cad:GFP (white in middle panels; green in bottom panels). Cyan dashed lines indicate clone boundaries. This clone becomes rounder over time (see D). (D) Circularity (solid lines) and number of divisions (dashed lines) versus time of a wt clone (red) and the *rasV12*^{UP} clone (blue) shown in C. (E) Mean ratio of final/initial clone circularity of wt and *rasV12*^{UP} clones. (F) Normalized Sqh:ChFP intensity at clone boundary (blue) and bulk junctions (red) in *rasV12*^{UP} and *myc*^{UP} clones. (G-J) Sqh:GFP (G,H) and D:GFP (I,J) localization in *myc*^{UP} (G,I) or *rasV12*^{UP} (H,J) clones. Yellow dots indicate mutant cells abutting wt cells. Sqh:GFP levels are reduced in *myc*^{UP} (G; quantified in F) whereas Sqh:GFP is enriched at clone boundaries of *rasV12*^{UP} (H, white arrowheads; quantified in F). D:GFP distribution and levels are unaffected in *myc*^{UP} (I), whereas D:GFP is enriched at some *rasV12*^{UP} clone boundaries (J, white arrowheads). In all graphs, **P*<0.05, ****P*<0.0005 (one-way ANOVA Tukey's test for A; one-way ANOVA Dunnett's test for B; *t*-test for E,F); *n*, clone numbers (A,E,F) or junction numbers (B); error bars represent s.d. Scale bars: 20 µm.

both boundary and bulk cell junction tensions need to be considered to fully account for segregation. This point is illustrated by the analysis of the mechanisms of clone rounding in the case of the Ft/Ds pathway where loss of Ft activity leads to change in cell junction tension both at the clone boundary and within the clone bulk.

We provide evidence that the rounding of *ft* clones can result from two apparently opposed mechanical inputs that require Dachs myosin activity. On one hand, the polarization of Ds at clone boundaries promotes Dachs polarity and increases junction tension. On the other hand, loss of Ft or Ds activity in the bulk of the clone leads to elevated Dachs levels and a decrease in junction tension. Our genetic and modeling findings show how these two distinct mechanical inputs both contribute to *ft* clone rounding. Importantly, increased levels of Dachs lead to an increased junction tension only at cell junctions where both Ds and Dachs are polarized, providing the first example of polarization and changes in the levels of a myosin leading to opposite changes in junction tension. The mechanism by which Dachs increases junction tension upon Ds-dependent polarization within tissues might be distinct from the one proposed for MyoII, because *in vitro* recombinant Dachs does not bind F-Actin in an ATP-dependent manner, but rather modulates F-Actin organization by promoting the binding of Zyxin to F-Actin (Cao et al., 2014). The mechanisms by which Dachs reduces tension inside *ft* and *ds* clones are independent of Ft and Ds activity and correlate with an increase of Dachs level. Dachs is reported to inhibit Wts by both Zyxin-dependent and -independent mechanisms (Rauskolb et al., 2011; Gaspar et al., 2015) and loss of Wts activity is associated with a similar decrease of cell junction tension. Wts is localized at cell-cell junction and its activity correlates with its binding to distinct partners and with distinct apical-basal distributions (Rauskolb et al., 2014; Sun et al., 2015). Whether these changes in Wts binding partner at cell-cell junctions can account for the regulation of tension by Dachs remains to be analyzed. Finally, the Ft/Ds pathway controls the shape of mammalian tissue (Saburi

Development (2016) 143, 623-634 doi:10.1242/dev.127993

et al., 2008), therefore it will be relevant to examine whether Ft and Ds regulate tissue shape in vertebrate systems through modulation of cell junction tension.

Our findings on the mechanisms of clone rounding provide information on cell competition and on a possible negative feedback between proliferation and tension regulation. In the context of cell competition, it has been recently reported that a clonal decrease of Myc levels, or a clonal increase of Myc levels in conjunction with an inhibition of apoptosis, promotes clone fragmentation and cell mixing; such cell-cell mixing increases cell-cell contacts and depends on reduced levels of F-actin, independently of changes in MyoII levels (Levayer et al., 2015). Our experimental results and previous findings show that Myc overexpression leads to clone rounding and a reduction of cell-cell contacts with neighboring wt cells (Prober and Edgar, 2002). Although we did not study Myc-mediated cell competition and our experimental setup was different from that of Levayer et al. (2015), it would be relevant to analyze whether Myc-mediated cell competition also depends on additional mechanisms associated with reduced cell-cell contact formation owing to a decrease of MyoII level. Lastly, our findings on Yki suggest the existence of a possible negative feedback between Yki activation and cell junction tension. Both experimental and modeling approaches converge to support the idea that mechanical tension is an important regulator of growth and proliferation (Shraiman, 2005; Hufnagel et al., 2007; Aegerter-Wilmsen et al., 2007, 2012; Mammoto and Ingber, 2010; Dupont et al., 2011; Sansores-Garcia et al., 2011; Aragona et al., 2013; Schluck et al., 2013; Rauskolb et al., 2014; Benham-Pyle et al., 2015). In particular, an increase in mechanical tensile stress leads to the activation of the Hippo/Yki (YAP/TAZ) pathway (Dupont et al., 2011; Sansores-Garcia et al., 2011; Rauskolb et al., 2014; Codelia et al., 2014). We have provided evidence that ectopic activation of the Hippo/Yki pathway in the notum epithelial tissue decreases junction tension in the bulk of the clone. The decrease of junction tension upon activation of Yki might unveil the possible existence of negative feedback from Hippo and Yki signaling in response to tensile stress in *Drosophila* tissues. Although the exact molecular mechanisms remain to be better characterized, we propose that such negative feedback could be instrumental to prevent prolonged activation of the Hippo and Yki pathways in response to an increase of mechanical tissue tension associated with tissue development or with external stress. Finally, by demonstrating that other signaling pathways regulate clone bulk or boundary tensions, we foresee that junction tension regulation might support cross-talk between tumor suppressor/proto-oncogene pathways and the Hippo/Yki pathways to define the size and shape of tissues and organs.

MATERIALS AND METHODS

Fly stocks

Drosophila stocks used were: ds^{05142}, $ft^{G\text{-}rv}$, ft^{8}, ft^{1}, d^{GC13}, d^{210}, UAS-ft^{RNAi}, UAS-sqh^{RNAi}, UAS-wts^{RNAi}, UAS-*yki*, UAS-*myc*, UAS-Ras^{V12} (see Table S1 for full genotypes and references). Clones were generated using FLP/FRT, flip-out or mosaic analysis with a repressible cell marker (MARCM) techniques (Xu and Rubin, 1993; Basler and Struhl, 1994; Lee and Luo, 1999). Clones were induced in second instar larvae (20 min heat-shock at 37°C) and analyzed 3-4 days later in 18-22 hAPF pupa. Live-imaging was carried out on ft^{RNAi} (*hs-flp;* $ft^{[G\text{-}rv]}$, *tub-GAL80*$^{[ts]}$*/AyGAL4; D:GFP, Baz:mChFP/UAS-*$ft^{[RNAi,\ JF03245]}$, *UAS-PH:ChFP*), *rasV12* (*hs-flp; UAS-ras*$^{[V12]}$*/E-Cad:GFP, tub-GAL80*$^{[ts]}$*; tub-FRT-GAL80-FRT-GAL4, UAS-mRFP*); clone induction and temperature changes are listed in the legend of Fig. 1 with further details in supplementary materials and methods. Their behaviors were compared with control clones: groups of 25-50 cells, with a circularity similar to that of ft^{RNAi} or $rasV12^{UP}$ clones at the onset of pupariation (10 hAPF), were tracked in a region of the epithelial tissue devoid of ft^{RNAi} clones (n=4) or in E-Cad:GFP pupae filmed at 29°C (n=4). Clones were analyzed in the anterior notum where the Ds and Fj gradients are absent and where cells undergo only one division (Bosveld et al., 2012).

Imaging, laser ablations, quantification of junction tension, and immunohistochemistry

Pupae were mounted and imaged at 25°C or 29°C using an inverted confocal spinning disk microscope (Nikon) (David et al., 2005). Time-lapse images were acquired every 10 min (0.5 µm/slice, 20-30 slices/z-stack). Images of live or fixed pupae were captured in 18-22 hAPF pupae.

Laser ablations were performed in 18-22 hAPF pupae using a Ti:Sapphire laser (Mai Tai DeepSee, Spectra Physics) and images were acquired using a two-photon laser-scanning microscope (LSM710 NLO, Carl Zeiss) in single-photon mode with bidirectional scan lasting 156 ms in a region of 18 µm x 18 µm (100×100 pixels) as previously described (Bosveld et al., 2012). Ablations were performed in tissues expressing D:GFP and Baz:mChFP (wt, *ft*, *ds*, *ds ft*), Ds:GFP and Baz:mChFP (wt, *dachs*), Baz:mChFP (*ft dachs*, *dachs*) or E-Cad:GFP (*ft*, *dachs*, *ds dachs*, *ds ft dachs*, myc^{UP}, yki^{UP}, $rasV12^{UP}$, sqh^{RNAi}, wts^{RNAi}, wts^{UP}, *ft* wts^{UP}). To determine the initial relaxation velocity, the vertex-vertex distance of the pre-cut and post-cut (two frames after ablation) junction was measured manually using ImageJ. For each given ablation, the relative uncertainty on the velocity measurement was of order of 5%, much lower than the biological variability between different ablation experiments.

For immunohistochemistry, pupae were dissected, fixed and stained as described by Ségalen et al. (2010). Primary antibodies used were rabbit anti-GFP (1:2000; A-11122, Molecular Probes) and mouse anti-FasIII (1:50; DSHB 7G10). Secondary antibodies were Cy3-conjugated donkey-anti-mouse (Jackson ImmunoResearch) and Alexa-488-conjugated goat-anti-rabbit (Molecular Probes). Images were collected with a confocal microscope (LSM710 NLO, Carl Zeiss).

Quantification of clone circularity

In the literature, the terms ‘circularity’, ‘compactness’, ‘segregation’ or ‘separation’ are used to express a size reduction of the contact with neighboring cells and can be quantified by measuring the clone area to square perimeter ratio ($C=4\pi\times\text{area}/\text{perimeter}^2$). C=1 for a circle. Circularity quantifications were performed on fixed and live tissues using membrane markers (mRFP, PH:ChFP, FasIII, Baz:mChFP, E-Cad:GFP) to delineate clone outlines. Clones were identified using loss (ubi-nlsGFP, ubi-H2B:RFP) or gain (UAS-GFP, UAS-mRFP, UAS-PH:ChFP) of expression. Clone outlines were manually drawn and measured using ImageJ.

Quantification of D:GFP polarity and junctional intensity of Sqh:ChFP/Sqh:GFP

D:GFP polarity was quantified by measuring on average projected images the D:GFP intensity at clone boundary junctions and transversal junctions within clones. The intensity was quantified manually (~10-40 transversal, ~20-60 boundary junctions per clone) and corrected by subtraction of the cytoplasmic signal. For each clone, the ratio between the average intensity at boundary junctions ($<I_{boundary}>$) and average intensity at transversal junctions ($<I_{transversal}>$) was determined. D:GFP is polarized when the ratio is >1. Junctional Sqh:ChFP or Sqh:GFP levels were quantified by manually measuring on average projected images the intensity on junctions inside clones, at clone boundaries as well as in wt junctions surrounding the clone. In each clone, ~15-50 boundary, bulk and wt junctions were measured. The intensities were corrected by subtraction of the cytoplasmic signals. Boundary and bulk junctional intensities were normalized to the wt junctional intensity to determine the average boundary and bulk intensities per clone.

Molecular biology, S2 cell culture and polarity assay

The Ubi-Dachs:mRFP transgene was generated by cloning a full length *dachs* cDNA (D isoform) into pUWR (DGRC) by Gateway cloning. Transgenesis was performed by Bestgene Inc. For the S2 cell polarity assay, the Ds intracellular domain was fused to the extracellular domain of echinoid

Development (2016) 143, 623-634 doi:10.1242/dev.127993

fused to mCherry (Ed:mCh:Ds:intra). The Ds intracellular fragment used in the S2 cell polarity assay was cloned into pMT:Ed:mCherry with a five-amino acid linker (GGGGS) between the mCherry and the Ds intracellular domain. Dachs was cloned into pUWG (DRGC). Induced cell polarity assays were carried out as described previously (Johnston et al., 2009; Ségalen et al., 2010). The polarization of the GFP-tagged Dachs construct relative to the induced Ed:mCh:Ds:intra polarity interface was quantified from single confocal scans as follows. The mean GFP intensities all around the cell cortex $I_{cell\text{-}cortex}$ and at the Ed:mCh:Ds:intra interface $I_{polarity\text{-}domain}$ were quantified blindly using ImageJ. The D:GFP was scored as polarized when the $I_{polarity\text{-}domain}/I_{cell\text{-}cortex}$ ratio was >1.1.

Theoretical analysis of clone shapes and numerical simulations

See supplementary materials and methods for theoretical analysis and numerical simulations.

Statistics

All error bars represent the standard deviation (s.d.). Statistical significance between experimental conditions was assessed using Student's *t*-tests: distribution normalities were checked using Kolmogorov–Smirnov test. In cases where the variances were different (*F*-test), significance was assessed using the unequal variance *t*-test. The one-way ANOVA Tukey's test was used to assess significance between genotypes within the same dataset (circularity, D:GFP polarity). Significance between either clone boundary or clone bulk tensions was assessed using one-way ANOVA Dunnett's test. By reporting significances based on one-way ANOVA, statistical differences between two different experimental conditions might have been missed.

Code availability

The code used for simulations based on the cellular Potts model is provided as a zip file in supplementary information along with the procedure to install and run it on MacOS.

Acknowledgements

We thank J. Axelrod, A. J. Bardin, S. Blair, J. Casal, Y. Hong, K. Irvine, E. Martin-Blanco, D. Pan, M. Simon, D. Strutt, N. Tapon, S. Tsukita, the Bloomington *Drosophila* Stock Center, Transgenic RNAi Project at Harvard Medical School, Vienna *Drosophila* RNAi Center, Developmental Studies Hybridoma Bank for reagents; PICT-IBiSA of the UMR3215 and U934 for assistance with microscopy; F. Elias, M. Durand, V. Leroy, C. Derec for discussions; and D. Lubensky, D. Pinheiro for comments.

Competing interests

The authors declare no competing or financial interests.

Author contributions

F.B. and Y.B. designed the project. F.B., I.B. and Z.W. performed experiments. Z.W. produced reagents. B.G. and M.R. wrote scripts to analyze data. F.B., B.G. and Y.B. analyzed the data. B.G. and F.G. developed the theoretical analysis. B.G. performed simulations. F.B., B.G., F.G. and Y.B. wrote the manuscript.

Funding

F.G. belongs to the CNRS research consortia (GdR) 'CellTiss' and 'MecaBio'. This work was supported by the Centre National de Recherche Scientifique (CNRS) , the Institut national de la santé et de la recherche médicale (INSERM), the Institut Curie, the labex DEEP and the following grants: ARC-4830, ANR-MorphoDro, ERC Starting (CePoDro), ERC Advanced (TiMorp), Programme Labellisé Fondation ARC [SL220130607097].

Supplementary information

Supplementary information available online at
http://dev.biologists.org/lookup/suppl/doi:10.1242/dev.127993/-/DC1

References

Adler, P. N., Charlton, J. and Liu, J. (1998). Mutations in the cadherin superfamily member gene dachsous cause a tissue polarity phenotype by altering frizzled signaling. *Development* **125**, 959-968.

Aegerter-Wilmsen, T., Aegerter, C. M., Hafen, E. and Basler, K. (2007). Model for the regulation of size in the wing imaginal disc of Drosophila. *Mech. Dev.* **124**, 318-326.

Aegerter-Wilmsen, T., Heimlicher, M. B., Smith, A. C., Barbier de Reuille, P., Smith, R. S., Aegerter, C. M. and Basler, K. (2012). Integrating force-sensing and signaling pathways in a model for the regulation of wing imaginal disc size. *Development* **139**, 3221-3231.

Aliee, M., Röper, J.-C., Landsberg, K. P., Pentzold, C., Widmann, T. J., Jülicher, F. and Dahmann, C. (2012). Physical mechanisms shaping the Drosophila dorsoventral compartment boundary. *Curr. Biol.* **22**, 967-976.

Ambegaonkar, A. A., Pan, G., Mani, M., Feng, Y. and Irvine, K. D. (2012). Propagation of Dachsous-Fat planar cell polarity. *Curr. Biol.* **22**, 1302-1308.

Aragona, M., Panciera, T., Manfrin, A., Giulitti, S., Michielin, F., Elvassore, N., Dupont, S. and Piccolo, S. (2013). A mechanical checkpoint controls multicellular growth through YAP/TAZ regulation by actin-processing factors. *Cell* **154**, 1047-1059.

Baena-Lopez, L. A., Baonza, A. and Garcia-Bellido, A. (2005). The orientation of cell divisions determines the shape of Drosophila organs. *Curr. Biol.* **15**, 1640-1644.

Baillon, L. and Basler, K. (2014). Reflections on cell competition. *Semin. Cell Dev. Biol.* **32**, 137-144.

Basler, K. and Struhl, G. (1994). Compartment boundaries and the control of Drosophila limb pattern by hedgehog protein. *Nature* **368**, 208-214.

Benham-Pyle, B. W., Pruitt, B. L. and Nelson, W. J. (2015). Cell adhesion. Mechanical strain induces E-cadherin-dependent Yap1 and β-catenin activation to drive cell cycle entry. *Science* **348**, 1024-1027.

Block, M., Schöll, E. and Drasdo, D. (2007). Classifying the expansion kinetics and critical surface dynamics of growing cell populations. *Phys. Rev. Lett.* **99**, 248101.

Bosch, J. A., Sumabat, T. M., Hafezi, Y., Pellock, B. J., Gandhi, K. D. and Hariharan, I. K. (2014). The Drosophila F-box protein Fbxl7 binds to the protocadherin Fat and regulates Dachs localization and Hippo signaling. *Elife* **3**, e03383.

Bosveld, F., Bonnet, I., Guirao, B., Tlili, S., Wang, Z., Petitalot, A., Marchand, R., Bardet, P.-L., Marcq, P., Graner, F. et al. (2012). Mechanical control of morphogenesis by Fat/Dachsous/four-jointed planar cell polarity pathway. *Science* **336**, 724-727.

Brittle, A. L., Repiso, A., Casal, J., Lawrence, P. A. and Strutt, D. (2010). Four-jointed modulates growth and planar polarity by reducing the affinity of dachsous for fat. *Curr. Biol.* **20**, 803-810.

Brittle, A., Thomas, C. and Strutt, D. (2012). Planar polarity specification through asymmetric subcellular localization of Fat and Dachsous. *Curr. Biol.* **22**, 907-914.

Brodland, G. W. (2002). The Differential Interfacial Tension Hypothesis (DITH): a comprehensive theory for the self-rearrangement of embryonic cells and tissues. *J. Biomech. Eng.* **124**, 188-197.

Calzolari, S., Terriente, J. and Pujades, C. (2014). Cell segregation in the vertebrate hindbrain relies on actomyosin cables located at the interhombomeric boundaries. *EMBO J.* **33**, 686-701.

Cao, Y., White, H. D. and Li, X.-D. (2014). Drosophila myosin-XX functions as an actin-binding protein to facilitate the interaction between Zyx102 and actin. *Biochemistry* **53**, 350-360.

Casal, J., Lawrence, P. A. and Struhl, G. (2006). Two separate molecular systems, Dachsous/Fat and Starry night/Frizzled, act independently to confer planar cell polarity. *Development* **133**, 4561-4572.

Chang, L.-H., Chen, P., Lien, M.-T., Ho, Y.-H., Lin, C.-M., Pan, Y.-T., Wei, S.-Y. and Hsu, J.-C. (2011). Differential adhesion and actomyosin cable collaborate to drive Echinoid-mediated cell sorting. *Development* **138**, 3803-3812.

Cho, E., Feng, Y., Rauskolb, C., Maitra, S., Fehon, R. and Irvine, K. D. (2006). Delineation of a Fat tumor suppressor pathway. *Nat. Genet.* **38**, 1142-1150.

Clark, H. F., Brentrup, D., Schneitz, K., Bieber, A., Goodman, C. and Noll, M. (1995). Dachsous encodes a member of the cadherin superfamily that controls imaginal disc morphogenesis in Drosophila. *Genes Dev.* **9**, 1530-1542.

Codelia, V. A., Sun, G. and Irvine, K. D. (2014). Regulation of YAP by mechanical strain through Jnk and Hippo signaling. *Curr. Biol.* **24**, 2012-2017.

David, N. B., Martin, C. A., Segalen, M., Rosenfeld, F., Schweisguth, F. and Bellaïche, Y. (2005). Drosophila Ric-8 regulates Galphai cortical localization to promote Galphai-dependent planar orientation of the mitotic spindle during asymmetric cell division. *Nat. Cell Biol.* **7**, 1083-1090.

Degoutin, J. L., Milton, C. C., Yu, E., Tipping, M., Bosveld, F., Yang, L., Bellaiche, Y., Veraksa, A. and Harvey, K. F. (2013). Riquiqui and minibrain are regulators of the hippo pathway downstream of Dachsous. *Nat. Cell Biol.* **15**, 1176-1185.

Donoughe, S. and DiNardo, S. (2011). dachsous and frizzled contribute separately to planar polarity in the Drosophila ventral epidermis. *Development* **138**, 2751-2759.

Dupont, S., Morsut, L., Aragona, M., Enzo, E., Giulitti, S., Cordenonsi, M., Zanconato, F., Le Digabel, J., Forcato, M., Bicciato, S. et al. (2011). Role of YAP/TAZ in mechanotransduction. *Nature* **474**, 179-183.

Fagotto, F. (2014). The cellular basis of tissue separation. *Development* **141**, 3303-3318.

Fagotto, F., Rohani, N., Touret, A.-S. and Li, R. (2013). A molecular base for cell sorting at embryonic boundaries: contact inhibition of cadherin adhesion by ephrin/Eph-dependent contractility. *Dev. Cell* **27**, 72-87.

Fernandez-Gonzalez, R., Simoes, S. d. M., Röper, J.-C., Eaton, S. and Zallen, J. A. (2009). Myosin II dynamics are regulated by tension in intercalating cells. *Dev. Cell* **17**, 736-743.

Development (2016) 143, 623-634 doi:10.1242/dev.127993

Garoia, F., Guerra, D., Pezzoli, M. C., López-Varea, A., Cavicchi, S. and García-Bellido, A. (2000). Cell behaviour of Drosophila fat cadherin mutations in wing development. *Mech. Dev.* **94**, 95-109.
Gaspar, P., Holder, M. V., Aerne, B. L., Janody, F. and Tapon, N. (2015). Zyxin antagonizes the FERM protein expanded to couple F-actin and Yorkie-dependent organ growth. *Curr. Biol.* **25**, 679-689.
Graner, F. (1993). Can surface adhesion drive cell-rearrangement? Part I: biological cell-sorting. *J. Theor. Biol.* **164**, 455-476.
Harvey, K. and Tapon, N. (2007). The Salvador-Warts-Hippo pathway - an emerging tumour-suppressor network. *Nat. Rev. Cancer* **7**, 182-191.
Heemskerk, I., Lecuit, T. and LeGoff, L. (2014). Dynamic clonal analysis based on chronic in vivo imaging allows multiscale quantification of growth in the Drosophila wing disc. *Development* **141**, 2339-2348.
Hilgenfeldt, S., Erisken, S. and Carthew, R. W. (2008). Physical modeling of cell geometric order in an epithelial tissue. *Proc. Natl. Acad. Sci. USA* **105**, 907.
Hufnagel, L., Teleman, A. A., Rouault, H., Cohen, S. M. and Shraiman, B. I. (2007). On the mechanism of wing size determination in fly development. *Proc. Natl. Acad. Sci. USA* **104**, 3835-3840.
Hutson, M. S., Tokutake, Y., Chang, M. S., Bloor, J. W., Venakides, S., Kiehart, D. P. and Edwards, G. S. (2003). Forces for morphogenesis investigated with laser microsurgery and quantitative modeling. *Science* **300**, 145-149.
Ishikawa, H. O., Takeuchi, H., Haltiwanger, R. S. and Irvine, K. D. (2008). Four-jointed is a Golgi kinase that phosphorylates a subset of cadherin domains. *Science* **321**, 401-404.
Johnston, L. A., Prober, D. A., Edgar, B. A., Eisenman, R. N. and Gallant, P. (1999). Drosophila myc regulates cellular growth during development. *Cell* **98**, 779-790.
Johnston, C. A., Hirono, K., Prehoda, K. E. and Doe, C. Q. (2009). Identification of an Aurora-A/PinsLINKER/Dlg spindle orientation pathway using induced cell polarity in S2 cells. *Cell* **138**, 1150-1163.
Justice, R. W., Zilian, O., Woods, D. F., Noll, M. and Bryant, P. J. (1995). The Drosophila tumor suppressor gene warts encodes a homolog of human myotonic dystrophy kinase and is required for the control of cell shape and proliferation. *Genes Dev.* **9**, 534-546.
Käfer, J., Hayashi, T., Marée, A. F. M., Carthew, R. W. and Graner, F. (2007). Cell adhesion and cortex contractility determine cell patterning in the Drosophila retina. *Proc. Natl. Acad. Sci. USA* **104**, 18549-18554.
Krieg, M., Arboleda-Estudillo, Y., Puech, P.-H., Käfer, J., Graner, F., Müller, D. J. and Heisenberg, C.-P. (2008). Tensile forces govern germ-layer organization in zebrafish. *Nat. Cell Biol.* **10**, 429-436.
Kuchen, E. E., Fox, S., Barbier de Reuille, P., Kennaway, R., Bensmihen, S., Avondo, J., Calder, G. M., Southam, P., Robinson, S., Bangham, A. et al. (2012). Generation of leaf shape through early patterns of growth and tissue polarity. *Science* **335**, 1092-1096.
Landsberg, K. P., Farhadifar, R., Ranft, J., Umetsu, D., Widmann, T. J., Bittig, T., Said, A., Jülicher, F. and Dahmann, C. (2009). Increased cell bond tension governs cell sorting at the Drosophila anteroposterior compartment boundary. *Curr. Biol.* **19**, 1950-1955.
Laplante, C. and Nilson, L. A. (2006). Differential expression of the adhesion molecule Echinoid drives epithelial morphogenesis in Drosophila. *Development* **133**, 3255-3264.
Lawrence, P. A. and Casal, J. (2013). The mechanisms of planar cell polarity, growth and the Hippo pathway: some known unknowns. *Dev. Biol.* **377**, 1-8.
Le Borgne, R., Bellaïche, Y. and Schweisguth, F. (2002). Drosophila E-cadherin regulates the orientation of asymmetric cell division in the sensory organ lineage. *Curr. Biol.* **12**, 95-104.
Lee, T. and Luo, L. (1999). Mosaic analysis with a repressible cell marker for studies of gene function in neuronal morphogenesis. *Neuron* **22**, 451-461.
Levayer, R., Hauert, B. and Moreno, E. (2015). Cell mixing induced by myc is required for competitive tissue invasion and destruction. *Nature* **524**, 476-480.
Ma, D., Yang, C.-H., McNeill, H., Simon, M. A. and Axelrod, J. D. (2003). Fidelity in planar cell polarity signalling. *Nature* **421**, 543-547.
Mahoney, P. A., Weber, U., Onofrechuk, P., Biessmann, H., Bryant, P. J. and Goodman, C. S. (1991). The fat tumor suppressor gene in Drosophila encodes a novel member of the cadherin gene superfamily. *Cell* **67**, 853-868.
Mammoto, T. and Ingber, D. E. (2010). Mechanical control of tissue and organ development. *Development* **137**, 1407-1420.
Mao, Y., Rauskolb, C., Cho, E., Hu, W.-L., Hayter, H., Minihan, G., Katz, F. N. and Irvine, K. D. (2006). Dachs: an unconventional myosin that functions downstream of Fat to regulate growth, affinity and gene expression in Drosophila. *Development* **133**, 2539-2551.
Mao, Y., Tournier, A. L., Bates, P. A., Gale, J. E., Tapon, N. and Thompson, B. J. (2011). Planar polarization of the atypical myosin Dachs orients cell divisions in Drosophila. *Genes Dev.* **25**, 131-136.
Marcinkevicius, E. and Zallen, J. A. (2013). Regulation of cytoskeletal organization and junctional remodeling by the atypical cadherin Fat. *Development* **140**, 433-443.
Matakatsu, H. and Blair, S. S. (2004). Interactions between Fat and Dachsous and the regulation of planar cell polarity in the Drosophila wing. *Development* **131**, 3785-3794.
Matakatsu, H. and Blair, S. S. (2008). The DHHC palmitoyltransferase approximated regulates Fat signaling and Dachs localization and activity. *Curr. Biol.* **18**, 1390-1395.
Matis, M. and Axelrod, J. D. (2013). Regulation of PCP by the Fat signaling pathway. *Genes Dev.* **27**, 2207-2220.
McGuire, S. E., Le, P. T. and Davis, R. L. (2001). The role of Drosophila mushroom body signaling in olfactory memory. *Science* **293**, 1330-1333.
Monier, B., Pélissier-Monier, A., Brand, A. H. and Sanson, B. (2010). An actomyosin-based barrier inhibits cell mixing at compartmental boundaries in Drosophila embryos. *Nat. Cell Biol.* **12**, 60-65; sup pp 1-9.
Patel, P. H. and Edgar, B. A. (2014). Tissue design: how Drosophila tumors remodel their neighborhood. *Semin. Cell Dev. Biol.* **28**, 86-95.
Prober, D. A. and Edgar, B. A. (2000). Ras1 promotes cellular growth in the Drosophila wing. *Cell* **100**, 435-446.
Prober, D. A. and Edgar, B. A. (2002). Interactions between Ras1, dMyc, and dPI3K signaling in the developing Drosophila wing. *Genes Dev.* **16**, 2286-2299.
Radszuweit, M., Block, M., Hengstler, J. G., Schöll, E. and Drasdo, D. (2009). Comparing the growth kinetics of cell populations in two and three dimensions. *Phys. Rev. E Stat. Nonlin. Soft. Matter Phys.* **79**, 051907.
Ranft, J., Basan, M., Elgeti, J., Joanny, J.-F., Prost, J. and Jülicher, F. (2010). Fluidization of tissues by cell division and apoptosis. *Proc. Natl. Acad. Sci. USA* **107**, 20863-20868.
Rauskolb, C., Pan, G., Reddy, B. V. V. G., Oh, H. and Irvine, K. D. (2011). Zyxin links fat signaling to the hippo pathway. *PLoS Biol.* **9**, e1000624.
Rauskolb, C., Sun, S., Sun, G., Pan, Y. and Irvine, K. D. (2014). Cytoskeletal tension inhibits Hippo signaling through an Ajuba-Warts complex. *Cell* **158**, 143-156.
Rauzi, M., Verant, P., Lecuit, T. and Lenne, P.-F. (2008). Nature and anisotropy of cortical forces orienting Drosophila tissue morphogenesis. *Nat. Cell Biol.* **10**, 1401-1410.
Resino, J., Salama-Cohen, P. and García-Bellido, A. (2002). Determining the role of patterned cell proliferation in the shape and size of the Drosophila wing. *Proc. Natl. Acad. Sci. USA* **99**, 7502-7507.
Restrepo, S., Zartman, J. J. and Basler, K. (2014). Coordination of patterning and growth by the Morphogen DPP. *Curr. Biol.* **24**, R245-R255.
Rodrigues-Campos, M. and Thompson, B. J. (2014). The ubiquitin ligase FbxL7 regulates the Dachsous-Fat-Dachs system in Drosophila. *Development* **141**, 4098-4103.
Röper, K. (2012). Anisotropy of Crumbs and aPKC drives myosin cable assembly during tube formation. *Dev. Cell* **23**, 939-953.
Saburi, S., Hester, I., Fischer, E., Pontoglio, M., Eremina, V., Gessler, M., Quaggin, S. E., Harrison, R., Mount, R. and McNeill, H. (2008). Loss of Fat4 disrupts PCP signaling and oriented cell division and leads to cystic kidney disease. *Nat. Genet.* **40**, 1010-1015.
Sansores-Garcia, L., Bossuyt, W., Wada, K.-I., Yonemura, S., Tao, C., Sasaki, H. and Halder, G. (2011). Modulating F-actin organization induces organ growth by affecting the Hippo pathway. *EMBO J.* **30**, 2325-2335.
Schluck, T., Nienhaus, U., Aegerter-Wilmsen, T. and Aegerter, C. M. (2013). Mechanical control of organ size in the development of the Drosophila wing disc. *PLoS ONE* **8**, e76171.
Ségalen, M., Johnston, C. A., Martin, C. A., Dumortier, J. G., Prehoda, K. E., David, N. B., Doe, C. Q. and Bellaïche, Y. (2010). The Fz-Dsh planar cell polarity pathway induces oriented cell division via Mud/NuMA in Drosophila and zebrafish. *Dev. Cell* **19**, 740-752.
Shraiman, B. I. (2005). Mechanical feedback as a possible regulator of tissue growth. *Proc. Natl. Acad. Sci. USA* **102**, 3318-3323.
Silva, E., Tsatskis, Y., Gardano, L., Tapon, N. and McNeill, H. (2006). The tumor-suppressor gene fat controls tissue growth upstream of expanded in the hippo signaling pathway. *Curr. Biol.* **16**, 2081-2089.
Simon, M. A., Xu, A., Ishikawa, H. O. and Irvine, K. D. (2010). Modulation of fat: dachsous binding by the cadherin domain kinase four-jointed. *Curr. Biol.* **20**, 811-817.
Sing, A., Tsatskis, Y., Fabian, L., Hester, I., Rosenfeld, R., Serricchio, M., Yau, N., Bietenhader, M., Shanbhag, R., Jurisicova, A. et al. (2014). The atypical cadherin fat directly regulates mitochondrial function and metabolic state. *Cell* **158**, 1293-1308.
Strutt, H. and Strutt, D. (2002). Nonautonomous planar polarity patterning in Drosophila: dishevelled-independent functions of frizzled. *Dev. Cell* **3**, 851-863.
Sun, S., Reddy, B. V. V. G. and Irvine, K. D. (2015). Localization of Hippo signalling complexes and Warts activation in vivo. *Nat. Commun.* **6**, 8402.
Umetsu, D., Aigouy, B., Aliee, M., Sui, L., Eaton, S., Jülicher, F. and Dahmann, C. (2014). Local increases in mechanical tension shape compartment boundaries by biasing cell intercalations. *Curr. Biol.* **24**, 1798-1805.
Wagstaff, L., Kolahgar, G. and Piddini, E. (2013). Competitive cell interactions in cancer: a cellular tug of war. *Trends Cell Biol.* **23**, 160-167.
Wartlick, O., Mumcu, P., Jülicher, F. and Gonzalez-Gaitan, M. (2011). Understanding morphogenetic growth control – lessons from flies. *Nat. Rev. Mol. Cell Biol.* **12**, 594-604.

Development (2016) 143, 623-634 doi:10.1242/dev.127993

Wei, S.-Y., Escudero, L. M., Yu, F., Chang, L.-H., Chen, L.-Y., Ho, Y.-H., Lin, C.-M., Chou, C.-S., Chia, W., Modolell, J. et al. (2005). Echinoid is a component of adherens junctions that cooperates with DE-Cadherin to mediate cell adhesion. *Dev. Cell* **8**, 493-504.

Willecke, M., Hamaratoglu, F., Kango-Singh, M., Udan, R., Chen, C.-L., Tao, C., Zhang, X. and Halder, G. (2006). The fat cadherin acts through the hippo tumor-suppressor pathway to regulate tissue size. *Curr. Biol.* **16**, 2090-2100.

Worley, M. I., Setiawan, L. and Hariharan, I. K. (2013). TIE-DYE: a combinatorial marking system to visualize and genetically manipulate clones during development in Drosophila melanogaster. *Development* **140**, 3275-3284.

Xu, T. and Rubin, G. M. (1993). Analysis of genetic mosaics in developing and adult Drosophila tissues. *Development* **117**, 1223-1237.

Zhao, B., Tumaneng, K. and Guan, K.-L. (2011). The Hippo pathway in organ size control, tissue regeneration and stem cell self-renewal. *Nat. Cell Biol.* **13**, 877-883.

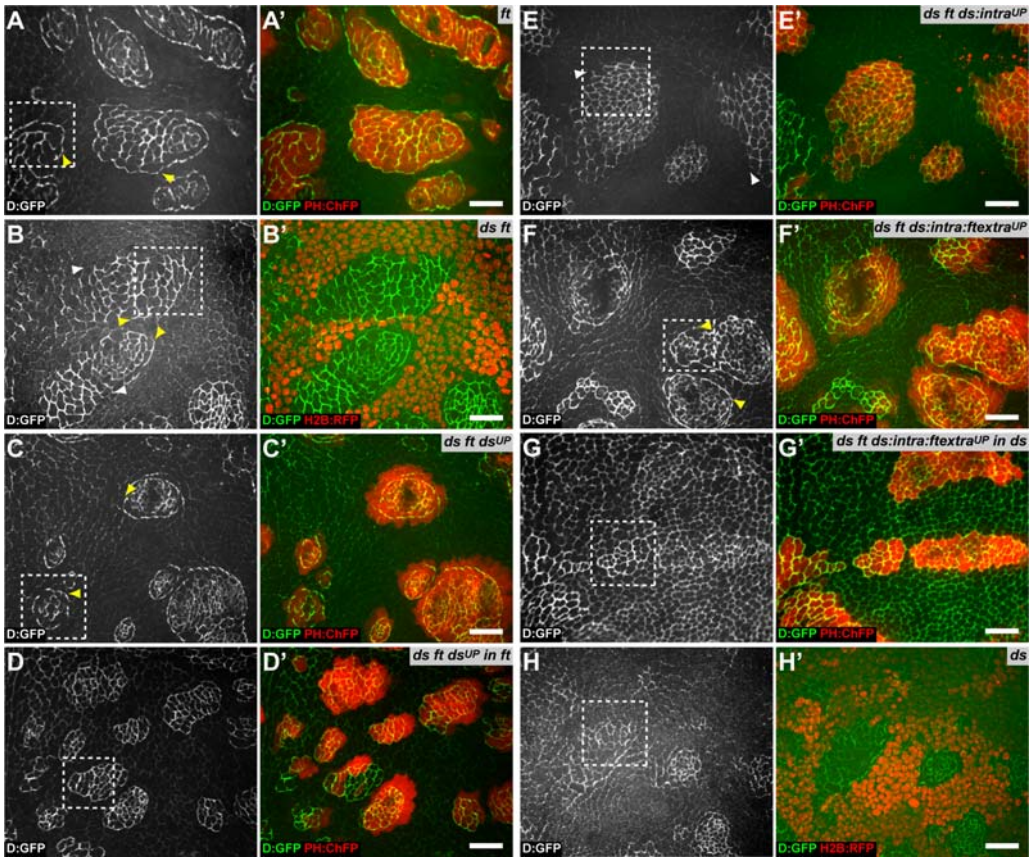

Fig. S1. D:GFP localization in mutant clones and tissues.

(**A-H'**) Confocal images of the localization of D:GFP in clones and tissues of the indicated genotypes. Anterior is to the right. Yellow arrowheads point at cells where D:GFP is polarized whereas white arrowheads indicate the ones which do not harbor polarization. Clones were identified by the absence of H2B:RFP nuclear marker (B', H') or by the presence of the PH:ChFP membrane marker (A', C'-G'). Boxed regions indicate the regions of the clone that are magnified in Fig. 2.

Genotypes are:

S1A : *hs-flp[22]; tub-Gal80[LL10], FRT40A/ ft[Gr-v], FRT40A; tub-Gal4[LL4], UAS-PH:ChFP*

S1B : *hs-flp[22]; ubi-H2B:RFP, FRT40A/ ds[05142], ft[Gr-v], FRT40A; D:GFP*

S1C : *hs-flp[22]; tub-Gal80[LL10], FRT40A/ ds[05142], ft[Gr-v], FRT40A; UAS-ds, D:GFP/ tub-Gal4[LL4], UAS-PH:ChFP*

S1D : *hs-flp[22]; ft[1], tub-Gal80[LL10], FRT40A/ ds[05142], ft[Gr-v], FRT40A; UAS-ds, D:GFP/ tub-Gal4[LL4], UAS-PH:ChFP*

S1E : *hs-flp[22]; tub-Gal80[LL10], FRT40A/ ds[05142], ft[Gr-v], FRT40A; UAS-ds:intra, D:GFP/ tub-Gal4[LL4], UAS-PH:ChFP*

S1F : *hs-flp[22]; tub-Gal80[LL10], FRT40A/ ds[05142], ft[Gr-v], FRT40A; UAS-ds:intra:ft:extra, D:GFP/ tub-Gal4[LL4], UAS-PH:ChFP*

S1G : *hs-flp[22]; ds[05142], tub-gal80[LL10], FRT40A/ ds[05142], ft[Gr-v], FRT40A; UAS-ds:intra:ft:extra, D:GFP/ tub-Gal4[LL4], UAS-PH:ChFP*

S1H : *hs-flp[22]; ubi-H2B:RFP, FRT40A/ ds[05142], FRT40A; D:GFP*

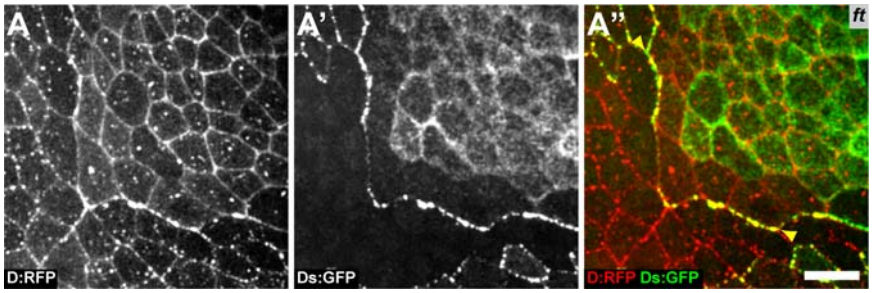

Fig. S2. Ds:GFP and D:RFP localization in *ft* clones.

(**A-A"**) Image of a *ft* clone in a tissue expressing D:RFP (white in A, red in A") and Ds:GFP (white in A', green in A"). Ds:GFP and D:RFP are polarized at the clone boundary (yellow arrowheads). Ds:GFP localization within the clone is more diffuse while D:RFP is still localized at cell-cell junctions. Previous results showed that Dachs membrane localization requires the DHHC palmitoyltransferase Approximated (Matakatsu and Blair, 2008). Therefore our findings suggest that while Ds is necessary to polarize the Dachs myosin, Ds is not required to target Dachs to the cell membrane. Note that the tissue neighboring the *ft* clone does not express Ds:GFP. Since the *ft*, *ds* and *ds:GFP* locus are one the same chromosome arm (2L), the generation of *ft ds:GFP* clones (*hs-flp[22]; FRT40A/ ds:GFP[44.2], ft[Gr-v], FRT40A; D:RFP*) results in a twin clone composed of wt cells (Ds:GFP negative cells). *ft* clones were identified by the increased expression of D:RFP, their circularity and the diffuse Ds:GFP localization. To illustrate the Ds polarization at the *ft* clone boundary we purposely show the boundary between *ft* cells and their wt Ds:GFP negative twins.
Scale bar: 10 µm.

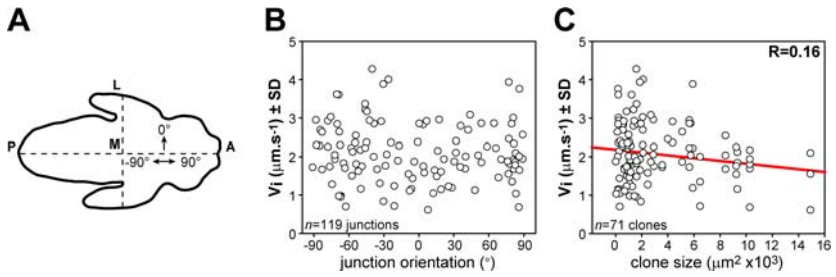

Fig. S3. *ft* clone boundary junction tension is independent of clone size and junction orientation.

(**A**) Sketch of a *Drosophila* pupa. Anterior-posterior (A-P) and medial-lateral axes (M-L) are indicated.

(**B**) Graph of the mean initial recoil velocity of vertices of ablated cell junctions at *ft* clone boundaries versus the orientation of the junction relative to the M-L axis (see panel A).

(**C**) Graph of the mean initial recoil velocity of vertices of ablated cell junctions at *ft* clone boundaries versus the clone size. The correlation score R is 0.16.

For graphs B and C the same data are plotted (119 ablations obtained from 71 different clones).

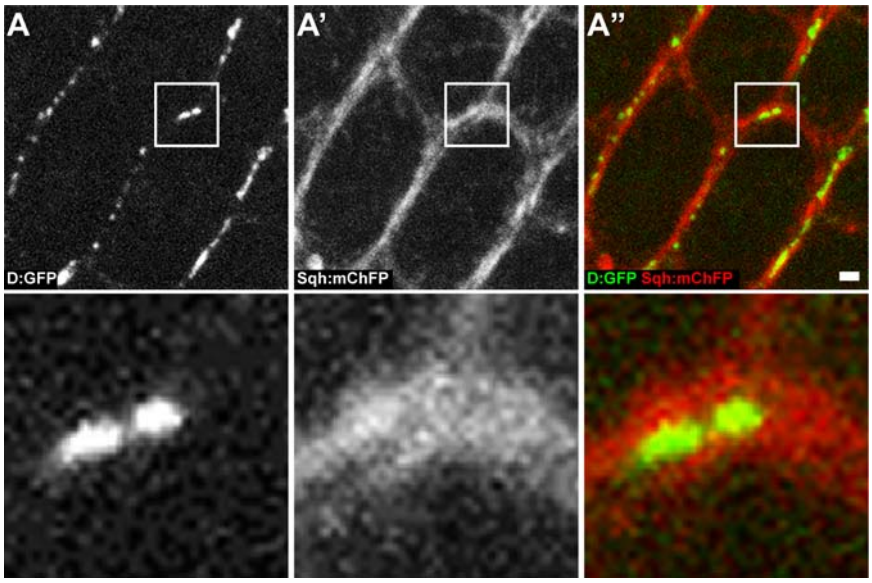

Fig. S4. Dachs myosin localizes in small clusters that do not colocalize with cortical MyoII.

(**A-A"**) Image of a tissue expressing D:GFP (white in A, green in A") and Sqh:mChFP (white in A', red in A"). The lower panels are magnifications of the boxed region. The images demonstrate that D:GFP localizes in small punctate structures at the cell membrane which do not colocalize with the cortical network of MyoII (Sqh:mChFP).

Scale bar: 1 μm.

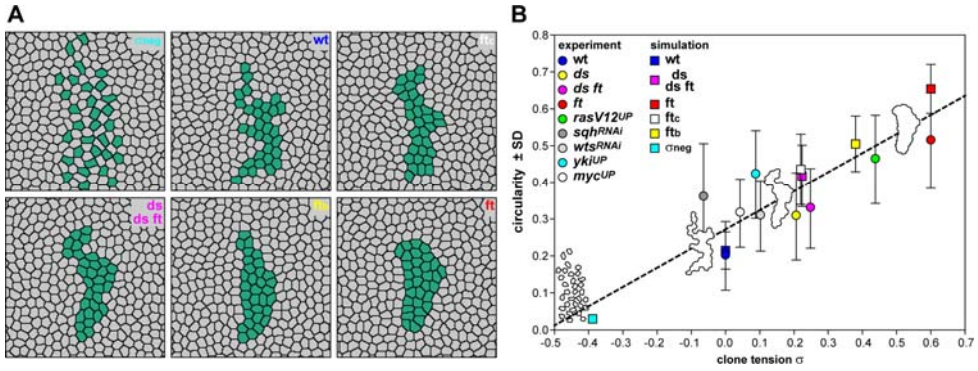

Fig. S5. Junction tensions at clone boundaries and inside clones contribute to clone rounding.

(**A**) Final shapes of six simulated mutant clones; from top left to bottom right: σ_{neg}; wt; ft_c; ds or ds ft; ft_b and ft. Simulated mutant conditions have been sorted in ascending order of their clone tension **σ**, which also corresponds to the ascending order of their final clone circularity (see panel B). In each simulation, the experimentally measured tension ratios γ_b/γ and γ_c/γ were used (see Supplementary Material). Simulating ft clones with junction tension solely reduced inside (ft_c), or solely increased at the clone boundary (ft_b) show that both effects are sufficient to induce clone rounding (the effect of the boundary tension being stronger), and when combined (ft) both contributions add up to achieve a stronger clone rounding. In the first panel (σ_{neg}), the clone tension is negative ($\sigma = -0.39$), illustrating a condition associated with clone scattering. This negative clone tension results from the swapping of γ_c and γ_b measured on *ft* clones, thus illustrating the respective role of γ_c and γ_b.

(**B**) Diagram showing the mean clone circularities C in the different experimental (circles) or simulation (squares) conditions versus dimensionless clone tension parameter σ. For each condition, 20 simulations were performed and thus 20 clones were quantified. Although there is no simple relationship between C and σ, two limits can nevertheless be considered: (i) for σ very large and positive, we expect C to get asymptotically closer to 1, corresponding to a perfectly circular clone; (ii) for σ very large and negative, we expect C to get closer to C_{min}, the latter being a threshold corresponding to the clone cells being completely scattered in the wt tissue ($C_{min} \approx 0.03$ from our ft[inv] simulation resulting in scattered clone). Nevertheless, for σ in the range 0 to 0.5, the circularity C seems to depend rather linearly on σ. We therefore add a linear fit of the experimental and simulated points plotted as a guide for the eye (dotted line): circularity $C \sim 0.5*(\sigma + 0.5)$. Some clone outlines obtained in (A) are added on the graph to illustrate the circularity of clones.

Movie 1. Time-lapse imaging of *ft*^{RNAi} clone.

The behavior of a *ft*^{RNAi} clone within the *Drosophila* anterior notum tissue recorded with 10 min intervals over a period of 30 h. Every cell of the tissue expresses Baz:mChFP (white, left panel and red, right panel) and D:GFP (white, middle panel and green, right panel), while the *ft*^{RNAi} cells also express PH-ChFP (white, left panel and red, right panel). The *ft*^{RNAi} clone accumulates D:GFP and rounds up.

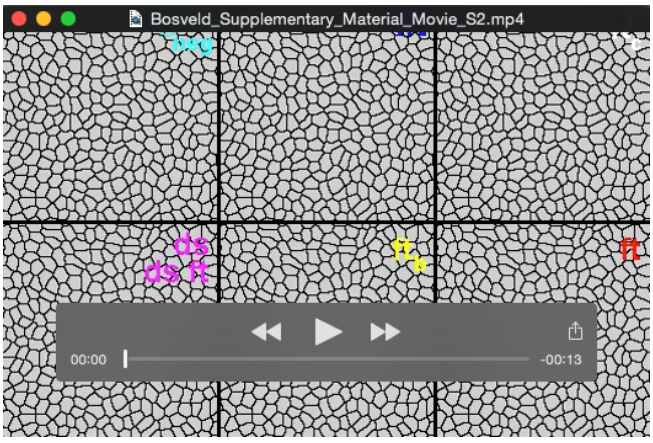

Movie 2: **Simulations showing the evolutions of six clones having different values of clone tension σ.**

Movies showing one simulation in each simulated mutant condition; from top left to bottom right: σ_{neg} (simulating hypothetical clones with inner tension γ_c and boundary tension γ_b respectively higher and lower than wt junction tension $\gamma_b < \gamma < \gamma_c$, namely $\gamma_b < \gamma < \gamma_c$, which results in negative a clone tension σ = -0.39, thereby illustrating a situation inverted with respect to our observed experimental *ft* and *ds*/*ds ft* clones where $\gamma_c < \gamma < \gamma_b$), wt, ft_c (simulating *ft* clones with junction tension solely reduced inside), ds or ds ft, ft_b (simulating *ft* clones with junction tension solely increased at the clone boundary) and ft. Simulated mutant conditions have been sorted in ascending order of their clone tensions **σ**, which also corresponds to the ascending order of their final clone circularities (supplementary material Fig. S5). In each simulation, the experimentally measured tension ratios γ_b/γ and γ_c/γ were used. Importantly, it is possible to run the exact same simulation up to the point where green cells with different junction properties appear, hence the identical initial clone shape in all six simulations (see supplementary movie). This is illustrated by reducing the frame rate of the movie at the time of appearance of the green cells. We mimicked the loss of activity of a given gene by suddenly modifying cell tensions in a group of cells (hence the appearance of green cells), arising from a same mother cell initially placed at the cluster center. The time of this modification was 9000 MCS, roughly corresponding to cells dividing three times to take into account the perdurance of the gene function. After the appearance of green cells, each clone evolves differently according to its own junction properties and clone tension σ, resulting in different final clone circularities. Because of the similarities of the γ_b values measured in *ds* and *ds ft* clones as well as the similarities of γ_c, their means were used for ds and ds ft simulations. As observed in the experiments (Fig. 1B), the shape of cells does not significantly change between the different simulations and clone rounding occurs via cell rearrangements. For each condition, 20 simulations were made and analysed to study clone circularity *in silico*.

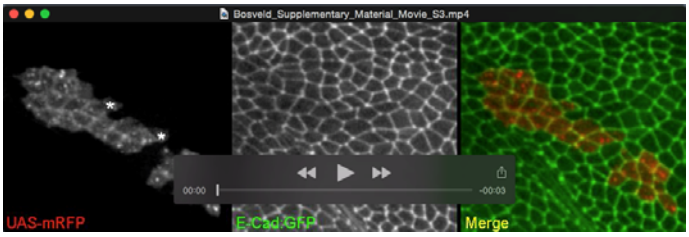

Movie 3: **Time-lapse imaging of *rasV12^{UP}* clone.**

The behavior of a *rasV12^{UP}* clone within the *Drosophila* anterior notum tissue recorded with 10 min intervals over a period of 17 h. The clone expresses mRFP (white, left panel and red, right panel), while every cell of the tissue expresses E-Cad:GFP (white, middle panel and green, right panel). The *rasV12^{UP}* clone rounds up in time. Note that some pI cells, which give rise to microchaetae (asterisks), segregate from the remaining of the clone via cell rearrangements.

Code availability

The code used for simulations based on the cellular Potts model is provided here as a zip file along with the procedure to install and run it on MacOS.

Click here to Download the zip

Supplementary Materials and Methods

Gal4/Gal80^{ts} gated clonal induction and imaging

Unless otherwise stated, somatic clones were induced in the second instar larval stage by heat shock (20 min at 37°C) and analyzed 3-4 days after clone induction in 18-22 hAPF pupae. The behavior of ft^{RNAi} somatic clones was analyzed in *hs-flp; ft$^{[G\text{-}rv]}$, tub-GAL80$^{[ts]}$/ AyGAL4; D:GFP, Baz:mChFP/ UAS-ft$^{[RNAi,\ JF03245]}$, UAS-PH:ChFP* and the behavior of *rasV12* gain of function clones in *hs-flp; UAS-ras$^{[V12]}$/ E-Cad:GFP, tub-GAL80$^{[ts]}$; tub-FRT-GAL80-FRT-GAL4, UAS-mRFP*. Clone induction and temperature changes were performed as follows. Embryos and larvae were raised at 18°C for 7 days. Upon a 7 min heat-shock at 37°C, which is sufficient to create one clone per hemi-notum, the second instar larvae were returned to 18°C. After 4-5 additional days at 18°C, late third instar larvae were transferred to 29°C to induce the expression of the *ft dsRNA*. After 22 ± 4 h at 29°C, the 10 hAPF old pupa were collected, mounted and imaged. Pupae harboring clones of 25-50 cells were selected and imaged for a period of 20-30 h at 29°C. Their behaviors were compared to control clones: groups of 25-50 cells, with a circularity similar to the ones of ft^{RNAi} or $rasV12^{UP}$ clones at the onset of pupariation (10 hAPF), were tracked in a region of the epithelial tissue devoid of ft^{RNAi} clones ($n = 4$) or in E-Cad:GFP pupae filmed at 29°C ($n = 4$). Clones were analyzed in the anterior region of the notum where the Ds and Fj gradients are absent and where cells undergo only one round of cell division (Bosveld et al., 2012).

Theoretical analysis of clone circularity

Theoretical analysis and numerical simulations are inspired by (Graner and Glazier, 1992;Graner, 1993;Bardet et al., 2013) that we adapt here for our specific questions. Several epithelial cellular organizations in *Drosophila* embryo, pupal wing and retina have been successfully described by minimizing an energy that balances adhesion between cells, cortex contractility and volume conservation (for review Morelli et al., 2012). Here, for simplicity, we consider the following energy to describe our 2D epithelium:

$$E = \sum_{\text{sides ij}} \gamma_{ij} l_{ij} + \sum_{\text{cells i}} \kappa_i (a_i - a_i^o)^2 \quad (1)$$

where γ_{ij} and l_{ij} are the line tension and length of the cell junction ij, respectively; κ_i is the compression modulus of cell i ensuring its volume conservation, namely that its area a_i remains close to its target value a_i^o. Note that the energy E displays only two terms: the first one, which can be experimentally probed by laser ablations of junctions, lumps all terms of different origins (adhesion, cortical contractility…) contributing to the full theoretical expression of cell junction tension (Käfer et al., 2007;Lecuit and Lenne, 2007;Rauzi et al., 2008;Hilgenfeldt et al., 2008;Bardet et al., 2013). We

observe that cell junctions are contractile, namely $\gamma_{ij} > 0$, and that the variability of their tensions is low. Their shrinkage is limited by area conservation described by the second term.

Here, we are interested in epithelia displaying two cell types, typically a clone of several mutant cells with different genetic and mechanical properties with respect to wt cells, surrounded by wt tissue, which constitutes our reference state of the tissue. We note γ the junction tension in the wt tissue, γ_c in the mutant clone, γ_b in junctions making up the interface boundary between wt and mutant cells. For simplicity we consider a tissue without boundary (e.g. with periodic boundary conditions), but what follows is readily generalizable to cells surrounded by a medium. Let us break down the energy E according to the two types of homotypic interfaces, and the heterotypic interface:

$$E = \gamma \sum_{ij} l_{ij} + \gamma_b \sum_{ij \in \mathrm{b}} l_{ij} + \gamma_c \sum_{ij \in \mathrm{c}} l_{ij} + \sum_{\text{cells i}} \kappa_i (a_i - a_i^o)^2$$

the first sum being made over wt junctions, the second one over junctions at the clone-wt interface boundary, and the third one over bulk clone junctions. Since we want to study the clone circularity as a function of the difference in cell mechanical properties, we define the perimeter of the clone-wt boundary P_b as $P_b = \sum_{ij \in b} l_{ij}$, and single it out in the energy. The perimeter of a cell reads $p_i = \sum_{<j>} l_{ij}$, the sum being made on cell neighbors. Noticing that $\sum_{\text{sides ij}} l_{ij} = \frac{1}{2} \sum_{\text{cells i}} p_i$, one can rewrite E :

$$E = \frac{\gamma}{2} \sum_i p_i + \frac{\gamma_c}{2} \sum_{i \in c} p_i + \tilde{\sigma} P_b + \sum_{\text{cells i}} \kappa_i (a_i - a_i^o)^2 \qquad \text{with} \qquad \tilde{\sigma} = \gamma_b - \frac{\gamma + \gamma_c}{2}$$

The two first terms are sums of perimeters over *all* cells in the wt tissue and *all* mutant cells in the clone, respectively, including those at the clone boundary. The third term, $\tilde{\sigma} P_b$, directly involves the clone perimeter P_b multiplied by $\tilde{\sigma}$, the difference between the heterotypic junction tension γ_b and the average of the two homotypic junction tensions γ, γ_c. This parameter represents the energy cost associated with the length of the clone boundary when junction tensions $(\gamma, \gamma_b, \gamma_c)$ are different, and vanishes for instance when all junction tensions are the same.

To better understand what $\tilde{\sigma}$ represents, let us consider a change in clone shape and perimeter δP_b that conserves the number of cells and leaves cell areas and perimeters unchanged, namely a change of clone shape only involving cell rearrangements and not changes in cell size and shape, as we observe experimentally. Those cell rearrangements that change clone boundary length P_b convert homotypic junctions into heterotypic junctions and vice versa. The corresponding change in energy then reads:

$$\delta E = \tilde{\sigma}\, \delta P_b$$

Therefore, $\tilde{\sigma} = \partial E / \partial P_b$ represents the energy cost per unit length of increasing the clone boundary length via cell rearrangement, namely the energy cost of turning homotypic junctions from wt and clone tissues into heterotypic boundary junctions. We call it the "clone line tension", not to be confused with the cell junction tension $\gamma_{ij} = \partial E / \partial l_{ij}$ that represents the energy cost per unit length of increasing junction *ij* length and that is probed with laser ablations. The sign and amplitude of $\tilde{\sigma}$ will therefore influence the evolution of the clone boundary toward a state of lower energy satisfying $\delta E < 0$:

$\tilde{\sigma} < 0 \Rightarrow \delta P_b > 0$: increase contact with neighbors favoring clone scattering

$\tilde{\sigma} > 0 \Rightarrow \delta P_b < 0$: decrease contact with neighbors favoring clone rounding

Consequently, taking wt tissue with junction tension γ as a reference, both an increase of junction tension at the clone boundary γ_b, or a decrease of junction tension within the clone γ_c, lead to $\tilde{\sigma} > 0$ and the rounding of the clone. In the last case $\tilde{\sigma} = 0$, which includes the case of a wt clone in a wt tissue, clone shapes have no line tension and their shape is fully determined by other factors. Since the wt tissue is our reference state, and because the initial recoil velocity of vertices of laser-ablated junctions v_{ij}^o measures only relative values of junction tensions ($v_{ij}^o = \mu\gamma_{ij}$, where μ is an unknown prefactor having the dimension of a friction coefficient) (Hutson et al., 2003;Farhadifar et al., 2007;Rauzi et al., 2008), we define the dimensionless clone line tension by $\sigma = \tilde{\sigma} / \gamma$, which reads:

(2) $$\sigma = \frac{1}{\gamma}\left(\gamma_b - \frac{\gamma + \gamma_c}{2}\right)$$

Note that experimental values of σ can therefore be directly estimated for each mutant condition by the ratios of recoil velocities after ablation: $\gamma_k/\gamma = v_k^o/v^o$, with *k* = *b*, *c*. The expression of σ is general and includes the particular case where the tensions on both sides of the clone boundary are the same, namely, $\gamma_c = \gamma$ (Landsberg et al., 2009).

This analysis provides us with qualitative predictions of the resulting clone circularities according to their junction mechanical properties, namely the values of $(\gamma_b/\gamma, \gamma_c/\gamma)$, and ultimately according to σ values.

Numerical simulations of clone circularity

The above simple theoretical analysis provides us with a qualitative trend of the clones to round up $(\sigma > 0)$, or in contrast to scatter $(\sigma < 0)$ according to the sign and amplitude of their dimensionless line tension σ that depends on the ratios $(\gamma_b/\gamma, \gamma_c/\gamma)$ [Eq. (2)]. To go further and actually try to link

more quantitatively the circularity of a growing and proliferating clone to its mechanical properties, we performed numerical simulations based on the energy given in Eq. (1) in a similar way to what was described in (Bardet et al., 2013). They were based on the Cellular Potts Model (CPM), which is relevant to describe variable cell shape, size, packing and irregular fluctuating interfaces (Graner and Glazier, 1992;Glazier and Graner, 1993;Mombach et al., 1995;Käfer et al., 2007;Marée et al., 2007;Krieg et al., 2008;Morelli et al., 2012). Like in experimental images, each cell was defined as a set of pixels, here on a 2D square lattice. The number of pixels defined the cell area, chosen to be comparable with experiments; an area term in the energy constrained this value [Eq. (1)]. We implemented for each cell tension the approximate value of retraction velocity actually measured in experiments, multiplied by 100 to deal with integer numbers for numerical convenience, namely $\gamma = 143, \gamma_b^{\mathrm{ft}} = 200, \gamma_c^{\mathrm{ft}} = 80, \gamma_b^{\mathrm{ds/ds,ft}} = 152, \gamma_c^{\mathrm{ds/ds,ft}} = 97$ and $\gamma_b^{\sigma_{\mathrm{neg}}} = 112, \gamma_c^{\sigma_{\mathrm{neg}}} = 191$. Note that in the simulations, given the very close values of γ_b an γ_c in *ds* and *ds,ft* clones, these two mutant conditions were simulated in a single set of simulations where the averages of γ_b an γ_c over *ds* and *ds,ft* mutant were used. In addition, to study the respective roles of increased clone boundary tension, decreased clone inner tension and their combination in clone rounding, we performed simulations where: (i) only the clone boundary tension was increased to γ_b^{ft} (condition $\mathrm{ft_b}$); (ii) only the clone inner tension was increased to γ_c^{ft} (condition $\mathrm{ft_c}$); (iii) the situation we observe experimentally in ft and ds/ds ft, namely higher clone boundary tension γ_b and lower clone inner tension γ_c was inversed, namely $\gamma_b < \gamma < \gamma_c$ (condition σ_{neg}), leading to a negative value of clone tension σ and clone scattering.

A cell shape changed when one of its pixels became attributed to one of the neighboring cells. The algorithm to minimize the energy *E* used Monte Carlo sampling and the Metropolis algorithm, as follows. We randomly drew (without replacement) a lattice pixel and one of its eight neighboring pixels. If both pixels belonged to different cells, we tried to copy the state of the neighboring pixel to the first one. If the copying decreased *E*, we accepted it, and if it increased *E*, we accepted it with probability $P = \exp(-\Delta E/T)$. Here ΔE was the difference in *E* before and after the considered copying. The prefactor *T* was a fluctuation allowance; it determined the extent of energy-increasing copy events, leading to membrane fluctuations (Mombach et al., 1995;Käfer et al., 2007). It had to be high enough to reduce pinning of the cell junctions on the pixel lattice, and low enough to keep the shape fluctuations close to the experimental ones. A reasonable compromise was obtained when *T* was of order of the junction tensions, and for numerical convenience we chose $T = 100$. We set the compression modulus $\kappa = 1$, and this last parameter could be varied over at least one order of magnitude barely changing the simulation outcomes.

We defined one Monte Carlo time step (MCS) as the number of random drawings equal to the number of lattice pixels. To simulate the growth and proliferation of somatic clones, we doubled the area of each cell over 3000 MCS, then divided it, mimicking the cell cycle which typically lasts 10 h in experiments. In order to mimic the variability of the division times, at the beginning of the simulations all cells were assigned at random a different stage of their cell cycle varying from 0% to 60% of cell cycle completion; and after each division, a random desynchronisation (0% to 20% of cell cycle completion) was introduced. To decrease possible effects of lattice anisotropy on cell shapes, we computed P and ΔE by including interactions up to the 20 next-nearest neighbors (Holm et al., 1991;Käfer et al., 2007).

To avoid possible effects of boundary condition anisotropy on clone shapes, we used periodic boundary conditions. Our field of simulation was a rectangle of 700 x 700 pixels. The cluster of cells was a circle of 700 pixels diameter inscribed in this square. All pixels out of this circle were assigned to external medium: a state without adhesion nor area and perimeter constraints. Cell-medium tension was arbitrarily assigned to $\gamma_0 = 200$ to be comparable with, but larger than, cell-cell tensions, thereby avoiding scattering of cells into the medium. During cluster growth due to rounds of cell growth and division, cells moving outwards and reaching the cluster boundary were transformed into medium. Thus, at each instant, the effective boundary conditions were that of a free circular cluster. Simulated clone images reported here are cropped 171 x 171 pixels zones. They do not exhibit any visible effect of boundary conditions and no direction appears privileged.

Such simulations enable to find a state of mechanical equilibrium of a group of cells that relaxes from an initial configuration of higher energy. Although they do not necessarily accurately describe the actual tissue dynamics leading to this equilibrium state, they are suitable to describe a quasi-static succession of mechanical equilibrium states. This is relevant here, where the cell number and area vary over time scales much slower than the time scale of mechanical relaxation.

We mimicked the loss of activity of a given gene by suddenly modifying cell tensions in a group of cells, arising from a same mother cell initially placed at the cluster center. The time of this modification was 9000 MCS, roughly corresponding to cells dividing three times to take into account the perdurance of the gene function. Although gene function perdurance is difficult to estimate and can vary, we estimated it to roughly 30 h (corresponding to three cell cycles of 10 hours) since in the ft^{RNAi} experiment the increase of D:GFP becomes apparent 30 h after the induction of ft^{RNAi}. For each tested mutant condition, 20 simulations were run with a different choice of the clone mother cell. For the wt, in the same simulation, 20 different mother cells were chosen. Since each simulation started with the

same seed for the random number generator, the only difference between wt and mutant simulations was the change in tension values.

When each cell had divided five times, roughly corresponding to 15000 MCS, we let the system evolve for a few more MCS to reach mechanical equilibrium. In order to compare the experimental and simulation data, the clone circularity was determined using the same method of measurements for experimental and simulated clones. Like in the experiments, we observed that the significant differences in the clone circularity were mainly due to the mutual arrangement of clone cells rather than to cell shape differences.

Table S1. Mutant alleles or transgenes used in this study.

Drosophila stock	Reference or Source
tub-FRT-GAL80-FRT-GAL4 UAS-*mRFP*	Gift from E. Martin-Blanco
E-Cad:GFP	Huang et al., 2009
ubi-*E-Cad:GFP*	Oda et al., 1998
Ds:GFP$^{44.2}$	Brittle et al., 2012
D:GFP	Bosveld et al., 2012
D:RFP	This study
ubi-*Baz:mChFP*	Bosveld et al., 2012
ubi-*H2B:RFP*	Bosveld et al., 2012
sqh-*sqh:GFP*	Royou et al., 2002
sqh-*sqh:ChFP*	Martin et al., 2008
UAS-*ds*	Matakatsu and Blair, 2004
UAS-*ds:intra*	Casal et al., 2006
UAS-*ds:intra:ft:extra*	Casal et al., 2006
dachs^{GC13}	Mao et al., 2006
dachs^{210}	Mao et al., 2006
ft^{1}	Mao et al., 2006
ft^{8}, *dachs*^{GC13}	Mao et al., 2006
ft$^{G\text{-}rv}$	Cho et al., 2006
UAS-*PH:ChFP*	Herszterg et al., 2013
UAS-*yki*	Huang et al., 2005
UAS-*ras*^{V12}	Karim and Rubin, 1998
UAS-*wts*	Feng and Irvine, 2007
hs-*flp*^{22}	Bloomington Stock Center
FRT40A	Bloomington Stock Center
ds^{05142}	Bloomington Stock Center
tub-*GAL4*^{LL4}	Bloomington Stock Center
tub-*GAL80*^{LL10}	Bloomington Stock Center
tub-*GAL80*^{ts10}	Bloomington Stock Center
UAS-*GFP*	Bloomington Stock Center
ubi-*nlsGFP*	Bloomington Stock Center
Act5C-FRT-*yellow*-FRT-*GAL4*^{25}	Bloomington Stock Center
UAS-*ft*$^{RNAi,\ TRiP.JF03245}$	Bloomington Stock Center, Ni et al., 2011
UAS-*dMyc*	Bloomington Stock Center
UAS-*wts*$^{RNAi,\ KK101055}$	VDRC Stock Center, Dietzl et al., 2007
UAS-*sqh*$^{RNAi,\ GD1695}$	VDRC Stock Center, Dietzl et al., 2007

Supplementary References

Bardet, P.L., Guirao, B., Paoletti, C., Serman, F., Léopold, V., Bosveld, F., Goya, Y., Mirouse, V., Graner, F., and Bellaïche, Y. (2013). PTEN Controls Junction Lengthening and Stability during Cell Rearrangement in Epithelial Tissue. Dev Cell *25*, 534-546.

Bosveld, F., Bonnet, I., Guirao, B., Tlili, S., Wang, Z., Petitalot, A., Marchand, R., Bardet, P.L., Marcq, P., et al. (2012). Mechanical Control of Morphogenesis by Fat/Dachsous/Four-Jointed Planar Cell Polarity Pathway. Science *336*, 724-27.

Brittle, A., Thomas, C., and Strutt, D. (2012). Planar polarity specification through asymmetric subcellular localization of Fat and Dachsous. Curr Biol *22*, 907-914.

Casal, J., Lawrence, P.A., and Struhl, G. (2006). Two separate molecular systems, Dachsous/Fat and Starry night/Frizzled, act independently to confer planar cell polarity. Development *133*, 4561-572.

Cho, E., Feng, Y., Rauskolb, C., Maitra, S., Fehon, R., and Irvine, K.D. (2006). Delineation of a Fat tumor suppressor pathway. Nat Genet *38*, 1142-150.

Dietzl, G., Chen, D., Schnorrer, F., Su, K.C., Barinova, Y., Fellner, M., Gasser, B., Kinsey, K., Oppel, S., et al. (2007). A genome-wide transgenic RNAi library for conditional gene inactivation in Drosophila. Nature *448*, 151-56.

Farhadifar, R., Röper, J.C., Aigouy, B., Eaton, S., and Jülicher, F. (2007). The Influence of Cell Mechanics, Cell-Cell Interactions, and Proliferation on Epithelial Packing. Curr Biol *17*, 2095-2104.

Feng, Y., and Irvine, K.D. (2007). Fat and expanded act in parallel to regulate growth through warts. Proc Natl Acad Sci U S A *104*, 20362-67.

Glazier, J.A., and Graner, F. (1993). Simulation of the differential adhesion driven rearrangement of biological cells. Phys Rev E *47*, 2128-154.

Graner, F. (1993). Can surface adhesion drive cell rearrangement? Part I: biological cell-sorting. J theor Biol *164*, 455-476.

Graner, F., and Glazier, J. (1992). Simulation of biological cell sorting using a two-dimensional extended Potts model. Phys Rev Lett *69*, 2013-2016.

Herszterg, S., Leibfried, A., Bosveld, F., Martin, C., and Bellaïche, Y. (2013). Interplay between the Dividing Cell and Its Neighbors Regulates Adherens Junction Formation during Cytokinesis in Epithelial Tissue. Dev Cell *24*, 256-270.

Hilgenfeldt, S., Erisken, S., and Carthew, R.W. (2008). Physical modeling of cell geometric order in an epithelial tissue. Proc Natl Acad Sci U S A *105*, 907.

Holm, E.A., Glazier, J.A., Srolovitz, D.J., and Grest, G.S. (1991). Effects of lattice anisotropy and temperature on domain growth in the two-dimensional Potts model. Phys Rev A *43*, 2662-68.

Huang, J., Wu, S., Barrera, J., Matthews, K., and Pan, D. (2005). The Hippo signaling pathway coordinately regulates cell proliferation and apoptosis by inactivating Yorkie, the Drosophila Homolog of YAP. Cell *122*, 421-434.

Huang, J., Zhou, W., Dong, W., Watson, A.M., and Hong, Y. (2009). Directed, efficient, and versatile modifications of the Drosophila genome by genomic engineering. Proc Natl Acad Sci U S A *106*, 8284-89.

Hutson, M.S., Tokutake, Y., Chang, M.S., Bloor, J.W., Venakides, S., Kiehart, D.P., and Edwards, G.S. (2003). Forces for morphogenesis investigated with laser microsurgery and quantitative modeling. Science *300*, 145-49.

Johnston, C.A., Hirono, K., Prehoda, K.E., and Doe, C.Q. (2009). Identification of an Aurora-A/PinsLINKER/Dlg spindle orientation pathway using induced cell polarity in S2 cells. Cell *138*, 1150-163.

Karim, F.D., and Rubin, G.M. (1998). Ectopic expression of activated Ras1 induces hyperplastic growth and increased cell death in Drosophila imaginal tissues. Development *125*, 1-9.

Käfer, J., Hayashi, T., Marée, A.F., Carthew, R.W., and Graner, F. (2007). Cell adhesion and cortex contractility determine cell patterning in the Drosophila retina. Proc Natl Acad Sci U S A *104*, 18549-554.

Krieg, M., Arboleda-Estudillo, Y., Puech, P.H., Käfer, J., Graner, F., Müller, D.J., and Heisenberg, C.P. (2008). Tensile forces govern germ-layer organization in zebrafish. Nat Cell Biol *10*, 429-436.

Landsberg, K.P., Farhadifar, R., Ranft, J., Umetsu, D., Widmann, T.J., Bittig, T., Said, A., Jülicher, F., and Dahmann, C. (2009). Increased cell bond tension governs cell sorting at the Drosophila anteroposterior compartment boundary. Curr Biol *19*, 1950-55.

Lecuit, T., and Lenne, P.F. (2007). Cell surface mechanics and the control of cell shape, tissue patterns and morphogenesis. Nat Rev Mol Cell Biol *8*, 633-644.

Mao, Y., Rauskolb, C., Cho, E., Hu, W.L., Hayter, H., Minihan, G., Katz, F.N., and Irvine, K.D. (2006). Dachs: an unconventional myosin that functions downstream of Fat to regulate growth, affinity and gene expression in Drosophila. Development *133*, 2539-551.

Marée, A.F.M., Grieneisen, V.A., and Hogeweg, P. (2007). The Cellular Potts Model and Biophysical Properties of Cells, Tissues and Morphogenesis. In Cell Based Models in Biology and Medicine (A.R.A. Anderson, M.A.J. Chaplain, and K.A. Rejniak, Birkhäuser Basel).

Martin, A.C., Kaschube, M., and Wieschaus, E.F. (2009). Pulsed contractions of an actin-myosin network drive apical constriction. Nature *457*, 495-499

Matakatsu, H., and Blair, S.S. (2004). Interactions between Fat and Dachsous and the regulation of planar cell polarity in the Drosophila wing. Development *131*, 3785-794.

Matakatsu, H., and Blair, S.S. (2008). The DHHC palmitoyltransferase approximated regulates Fat signaling and Dachs localization and activity. Curr Biol *18*, 1390-95.

Mombach, J.C., Glazier, J.A., Raphael, R.C., and Zajac, M. (1995). Quantitative comparison between differential adhesion models and cell sorting in the presence and absence of fluctuations. Phys Rev Lett *75*, 2244-47.

Morelli, L.G., Uriu, K., Ares, S., and Oates, A.C. (2012). Computational approaches to developmental patterning. Science *336*, 187-191.

Ni, J.Q., Zhou, R., Czech, B., Liu, L.P., Holderbaum, L., Yang-Zhou, D., Shim, H.S., Tao, R., Handler, D., et al. (2011). A genome-scale shRNA resource for transgenic RNAi in Drosophila. Nat Methods *8*, 405-07.

Oda, H., Tsukita, S., and Takeichi, M. (1998). Dynamic behavior of the cadherin-based cell-cell adhesion system during Drosophila gastrulation. Dev Biol *203*, 435-450.

Rauzi, M., Verant, P., Lecuit, T., and Lenne, P.F. (2008). Nature and anisotropy of cortical forces orienting Drosophila tissue morphogenesis. Nat Cell Biol *10*, 1401-410.

Royou, A., Sullivan, W., and Karess, R. (2002). Cortical recruitment of nonmuscle myosin II in early syncytial Drosophila embryos: its role in nuclear axial expansion and its regulation by Cdc2 activity. J Cell Biol *158*, 127-137.

Ségalen, M., Johnston, C.A., Martin, C.A., Dumortier, J.G., Prehoda, K.E., David, N.B., Doe, C.Q., and Bellaïche, Y. (2010). The Fz-Dsh planar cell polarity pathway induces oriented cell division via Mud/NuMA in Drosophila and zebrafish. Dev Cell *19*, 740-752.